ISME

M. Garousi*
M.Sc. Student

A. Khaleghi†
Assistant Professor

M. Nazari‡
Associate Professor

Simultaneous Estimation of Heat Fluxes Applied to the Wall of a Channel with Turbulent Flow using Inverse Analysis

The main purpose of this study is to estimate the step heat fluxes applied to the wall of a two-dimensional symmetric channel with turbulent flow. For inverse analysis, conjugate gradient method with adjoint problem is used. In order to calculate the flow field, SST $k-\omega$ two equation model is used. In this study, adjoint problem is developed to conduct an inverse analysis of heat transfer in a channel turbulent fluid flow. The primary purpose is to find suitable number of sensors at each half of the channel's wall and an appropriate space on the wall for locating the sensors. The innovate aspect of the study is to find out ideal length of the channel's wall on which sensors are located.

Keywords: Inverse analysis, Conjugate gradient method, Turbulent flow, Heat flux estimation

1 Introduction

Inverse heat transfer problems rely on temperature or heat flux measurements to estimate unknown quantities in physical problems analysis relating to Thermal Engineering. For example, inverse conduction problems generally relate to the estimation of unknown heat flux applied to a boundary with the help of temperature measurements taken below the boundary's surface. Although in classic direct heat transfer problems, the cause (boundary heat flux) is known and the effect (temperature field) is unknown, inverse problems involve estimating the cause with the knowledge of the effect.

In spite of the fact that most of the initial researches on inverse heat transfer were related to pure conduction problems, the attention of interested researchers into the subject has been attracted to conduction-convection problems in recent years. Huang and Chen [1] came up with a solution to an inverse problem in a three-dimensional channel flow forced convection, in order to estimate the wall heat flux using conjugate gradient method. The effects of channel's height, fluid's velocity at the inlet of the channel, and measurement errors on the results of inverse analysis were discussed in their study. Li and Yan [2] analysed an inverse convection problem, in order to determine the wall heat flux in a circular channel.

* M.Sc. Student, Faculty of Mechanical and Mechatronics Engineering, Shahrood University of Technology, Shahrood, Iran, morteza.garousi@yahoo.com

† Corresponding Author, Assistant Professor, Faculty of Mechanical and Mechatronics Engineering, Shahrood University of Technology, Shahrood, Iran, khaleghi@shahroodut.ac.ir

‡Associate Professor, Faculty of Mechanical and Mechatronics Engineering, Shahrood University of Technology, Shahrood, Iran, mnazari@shahroodut.ac.ir

Receive : 2018/12/20 Accepted : 2019/07/14

In their study, the impacts of the functional form of the wall heat flux, the number of measurement points, and measurement errors on inverse analysis were examined. Orlande and Colaco [3] addressed an inverse forced convection problem for the purpose of simultaneously estimating boundary heat fluxes in channels with irregular shapes. In their research, three different types of heat flux (1-temporally dependant 2-spatially dependant 3-temporally and spatially dependant) were estimated with conjugate gradient method. Prud'homme and Nguyen [4] solved inverse free convection problems using conjugate gradient method, in order to scrutinise the effects of Rayleigh number. For the purpose of determining temporally and spatially dependant heat flux applied to the wall of an enclosure, they placed the sensors needed for inverse analysis inside the flow field.

The results of their study indicated it would be possible to find solutions for Rayleigh numbers much bigger than the Rayleigh numbers considered in the previous researches, if the sensors were replaced near to the active boundary. Kim et al. [5] analysed a nonlinear inverse convection problem with the help of sequential gradient method. The fluid flow between two parallel plates was considered to be laminar in their study. In order to estimate the heat flux applied to one of the plates, they used sequential gradient method and temperature measurements from the other insulated plate. Kim and Lee [6] determined thermophysical properties of laminar fluid flow inside a circular channel using an inverse method. Their proposed inverse method could estimate thermal conductivity and heat capacity of the fluid of interest. Hong and Baek [7] conducted an inverse analysis for the purpose of estimating transient temperature distribution at the inlet of a channel with two-phase laminar flow. In their research, conjugate gradient method and Tikhonov regularisation were utilised. They examined the effects of functional form of the inlet temperature profile, number of measurement points, and measurement errors on the results.

Chen et al. [8] compared application of whole-domain and sequential function specification methods in an inverse problem relating to transient conjugate heat transfer in laminar forced convection inside a circular channel. In their study, the above-mentioned inverse methods were used to simultaneously estimate inlet temperature and wall heat flux profiles. The results of their research showed that the estimations achieved with the help of whole-domain specification method are slightly more accurate than those obtained by sequential function specification method. Lin et al. [9] analysed an inverse problem concerning transient forced convection in parallel plate channels. In their study, heat flux profile applied to the channel's wall was determined using conjugate gradient method. Their results showed that heat flux estimation depends heavily upon sensor's location and plate's thickness. Zhao et al. [10] calculated heat flux profile applied to the wall of a two-dimensional enclosure with ventilation ports. Mixed convection inside the enclosure was considered in their study. The results of their research indicated that the accuracy of estimated wall heat flux is highly affected by Reynolds number and functional form of the heat flux.

Furthermore, the effects of measurement errors were examined in their study. Zhao et al. [11] managed to estimate heat flux profiles applied to the boundary of an enclosure containing a conducting solid block using conjugate gradient method. In their research, the effects of Rayleigh number, size, and thermal conductivity of the solid block were scrutanised. Parwani et al. [12] calculated inlet temperature profile of a laminar parallel plate channel flow with the help of conjugate gradient method with adjoint problem. The results of their study showed good agreement between exact and estimated temperature profiles at the inlet of the channel. Moghadassian and Kowsary [13] analysed a boundary design inverse problem relating to the combination of radiation and natural convection inside a two-dimensional enclosure numerically. In order to carry out an inverse analysis, they used Levenberg-Marquardt method and for the purpose of calculating the elements of the sensitivity matrix, Broyden's method was applied in their research.

Moreover, they utilised finite volume method to numerically solve direct problem, governing equations of the fluid flow, and radiation equations. The principal objective of their research was to obtain heaters' strength in order to produce temperature and heat flux distributions on the design surface. The results of their study indicated good agreement between estimated and desired heat fluxes and what's more, maximum value of root-mean-square error was less than 1%. Zhang et al. [14] studied an inverse heat transfer problem in a rectangular enclosure containing a solid obstacle. Heat transfer mechanisms considered in their research were conduction and natural convection and also radiation between internal surfaces of the enclosure was neglected. Additionally, Reynolds number of the fluid flow was within laminar range in their study. They could obtain reasonably accurate estimations of heat flux profiles applied to vertical walls of the enclosure using conjugate gradient method and simulated temperature measurements. Min et al. [15] considered an inverse convection heat transfer in a two–dimensional channel mounted with square ribs in their work.

A simplified conjugate gradient method was adopted for optimising the convection heat transfer. The optimal pitch ratio of the ribs was searched under the maximum heat transfer rate. The sensitivity and adjoint problems were not considered but a constant search step size was applied. The results of their work showed that the simplified conjugate gradient method can be used to search the optimal pitch ratio of the ribs at various initial values, but the constant search step size may result in the oscillation of the numerical results. Furthermore, the searched optimal pitch ratio in their work with the help of inverse method at one Reynolds number could be spread to a large range of Reynolds numbers. Bangian-Tabrizi and Jaluria [16] developed a method based on a search and optimisation approach to solve the inverse natural convection problem of a two-dimensional heat source on a vertical flat plate. Their inverse problem involved determination of the strength and location of the heat source, which was taken as a fixed-length region of the wall with an isothermal or isoflux condition, by employing a few selected data points downstream. This was achieved by numerical simulations of the region at differing source strengths and locations, thus obtaining relevant temperature interpolation functions of source location and strength for selected data points.

A search based optimisation method, particle swarm optimisation (PSO), was then applied to find the best pair of vertical locations for input of data. The goal of their method was to reduce the uncertainty and approach essentially unique solutions. The error of the method was found to be acceptable for both source strength and location.

Hafid and Lacroix [17] predicted the time-varying protective bank coating the internal surface of the refractory brick walls of a melting furnace. An inverse heat transfer procedure was presented for predicting simultaneously operating and thermal parameters of a melting furnace. These parameters were the external heat transfer coefficient, the thermal conductivity of the phase change material (PCM) and the time-varying heat load of the furnace. Once these parameters were estimated, the time-varying protective PCM bank could be predicted. The melting and solidification of the PCM were modeled with the enthalpy method. The inverse problem was handled with the Levenberg-Marquardt Method (LMM) combined to the Broyden method (BM). The models were validated and the effect of the position of the temperature sensor embedded in the furnace wall, of the data capture frequency and of the measurement noise, was investigated. A statistical analysis for the parameter estimation was also carried out. Analysis of the results yielded recommendations concerning the location of the embedded sensor and the data capture frequency.

The aforesaid review makes it clear that the main gap within the domain of inverse convection is the lack of sufficient studies concerning turbulent convection. There are various methods of solving an inverse problem, but conjugate gradient method (CGM) with adjoint problem is used in this study. Main advantage of the above-mentioned method is that it has no need of calculating sensitivity matrix which is a time-consuming process.

Most of the previous studies on inverse heat transfer are restricted to pure conduction or laminar convection. The main innovate aspect of the present study is to find out optimum space on the channel's wall for locating the sensors in order to estimate the heat fluxes as accurate as possible.

2 Physical problem and steady state flow field formulations

The physical problem under consideration in this paper involves forced turbulent convection inside a two-dimensional symmetric channel, such as the one shown in Figure (1). Flow field is assumed to be in steady state for the sake of computational effort and Reynolds number at the inlet of the channel is within turbulent range ($Re_{in} = 10^4$). The length of the channel is taken long enough to ensure fully-developed state ($L = 8\,m$). The height of the channel ($2r_0$) is equal to 0.1m and also the fluid is taken to be water in this paper.
In order to validate the steady state flow field, which is calculated in this paper numerically, steady state temperature field is also obtained for the purpose of working out steady state Nusselt number in the fully-developed region of the channel using pseudo-transient approach. The set of governing equations to calculate steady state flow field relating to the physical problem depicted in Figure (1) are,

$$\frac{\partial}{\partial x}(\rho u) + \frac{\partial}{\partial y}(\rho v) = 0 \tag{1}$$

$$\frac{\partial}{\partial x}(\rho uu) + \frac{\partial}{\partial y}(\rho vu) = \frac{\partial}{\partial x}\left(\mu_{eff}\frac{\partial u}{\partial x}\right) + \frac{\partial}{\partial y}\left(\mu_{eff}\frac{\partial u}{\partial y}\right) - \frac{\partial p}{\partial x} - \frac{2}{3}\frac{\partial}{\partial x}(\rho k) + \frac{\partial}{\partial x}\left(\mu_t\frac{\partial u}{\partial x}\right) + \frac{\partial}{\partial y}\left(\mu_t\frac{\partial v}{\partial x}\right) \tag{2}$$

$$\frac{\partial}{\partial x}(\rho uv) + \frac{\partial}{\partial y}(\rho vv) = \frac{\partial}{\partial x}\left(\mu_{eff}\frac{\partial v}{\partial x}\right) + \frac{\partial}{\partial y}\left(\mu_{eff}\frac{\partial v}{\partial y}\right) - \frac{\partial p}{\partial y} - \frac{2}{3}\frac{\partial}{\partial y}(\rho k) + \frac{\partial}{\partial y}\left(\mu_t\frac{\partial v}{\partial y}\right) + \frac{\partial}{\partial x}\left(\mu_t\frac{\partial u}{\partial y}\right) \tag{3}$$

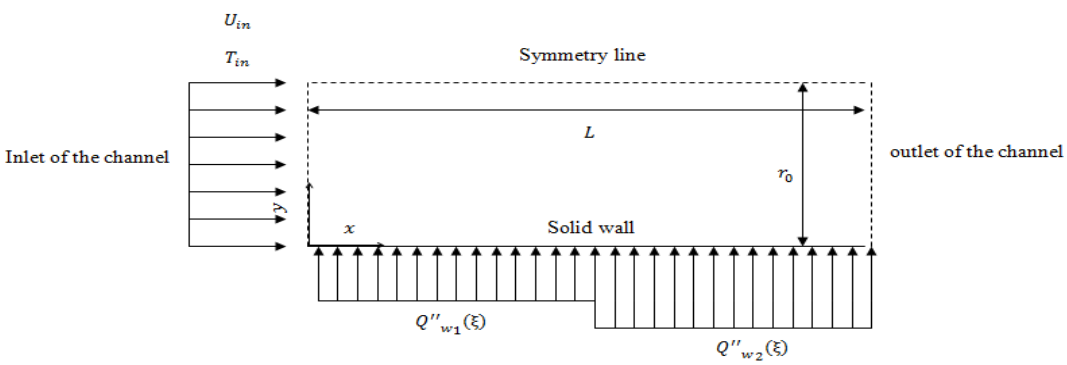

Figure 1 The physical problem under consideration.

Eqs. (1)-(3) are respectively called mass, x-momentum, and, y-momentum conservations in the Cartesian coordinates. The variable μ_{eff} denotes effective viscosity which is calculated as follows:

$$\mu_{eff} = \mu_t + \mu \tag{4}$$

It should be noted that Eqs. (1)-(3) are called the Reynolds-Averaged Navier-Stocks (RANS) equations and u and v are the time-average velocity components [18]. In order to calculate the variables k (turbulence kinetic energy) and μ_t (eddy viscosity), $SST\ k-\omega$ two-equation turbulence model is used in this paper. The reason behind the decision is the model's high performance at resolving near-wall regions. The governing equations in this model are [19],

$$\frac{\partial}{\partial x}(\rho u k) + \frac{\partial}{\partial y}(\rho v k) = \frac{\partial}{\partial x}\left(\mu_1 \frac{\partial k}{\partial x}\right) + \frac{\partial}{\partial y}\left(\mu_1 \frac{\partial k}{\partial y}\right) - \beta^* \rho \omega k + \tau_{mn}\frac{\partial u_m}{\partial x_n} \tag{5}$$

$$\frac{\partial}{\partial x}(\rho u \omega) + \frac{\partial}{\partial y}(\rho v \omega) = \frac{\partial}{\partial x}\left(\mu_2 \frac{\partial k}{\partial x}\right) + \frac{\partial}{\partial y}\left(\mu_2 \frac{\partial k}{\partial y}\right) - \beta \rho \omega^2 + \frac{\rho\gamma}{\mu_t}\tau_{mn}\frac{\partial u_m}{\partial x_n} + 2(1 - F_1)\rho\sigma_{\omega 2}\frac{1}{\omega}\frac{\partial k}{\partial x_m}\frac{\partial \omega}{\partial x_m} \tag{6}$$

The parameters used in Eqs. (5)-(6) could be obtained as follows [19],

$$\tau_{mn} = \mu_t\left(\frac{\partial u_m}{\partial x_n} + \frac{\partial u_n}{\partial x_m}\right) - \frac{2}{3}\rho k \delta_{mn} \tag{7}$$

$$\delta_{mn} = \begin{cases} 1 & , m = n \\ 0 & , m \neq n \end{cases} \tag{8}$$

$$\mu_1 = \mu + \sigma_k \mu_t \qquad \mu_2 = \mu + \sigma_\omega \mu_t \tag{9}$$

$$\sigma_k = F_1\sigma_{k1} + (1-F_1)\sigma_{k2} \qquad \sigma_\omega = F_1\sigma_{\omega 1} + (1-F_1)\sigma_{\omega 2} \tag{10}$$

$$\gamma = F_1\gamma_1 + (1-F_1)\gamma_2 \qquad \beta = F_1\beta_1 + (1-F_1)\beta_2 \tag{11}$$

$$\sigma_{k1} = 0.85 \quad \sigma_{k2} = 1.0 \quad \sigma_{\omega 1} = 0.5 \quad \sigma_{\omega 2} = 0.856 \quad \beta_1 = 0.075 \quad \beta_2 = 0.0828 \tag{12}$$

$$\gamma_1 = \frac{\beta_1}{\beta^*} - \frac{\sigma_{\omega 1}\kappa^2}{\sqrt{\beta^*}} \qquad \gamma_2 = \frac{\beta_2}{\beta^*} - \frac{\sigma_{\omega 2}\kappa^2}{\sqrt{\beta^*}} \tag{13}$$

$$\beta^* = 0.09 \quad \kappa = 0.41 \tag{14}$$

$$F_1 = tanh({arg_1}^4) \tag{15}$$

$$arg_1 = min\left[max\left(\frac{\sqrt{k}}{0.09\omega y}; \frac{500\nu}{y^2\omega}\right); \frac{4\rho\sigma_{\omega 2}k}{CD_{k\omega}y^2}\right] \tag{16}$$

$$CD_{k\omega} = max\left(2\rho\sigma_{\omega 2}\frac{1}{\omega}\frac{\partial k}{\partial x_j}\frac{\partial \omega}{\partial x_j}; 10^{-20}\right) \tag{17}$$

According to $SST\ k-\omega$ two-equation turbulence model, eddy viscosity is calculated by the following relations [19],

$$\mu_t = \frac{\rho a_1 k}{max(a_1\omega; \Omega F_2)} \tag{18}$$

$$a_1 = 0.31 \tag{19}$$

$$\Omega = \sqrt{2\Omega_{ij}\Omega_{ij}} \qquad \Omega_{ij} = \frac{1}{2}\left(\frac{\partial u_i}{\partial x_j} - \frac{\partial u_j}{\partial x_i}\right) \tag{20}$$

$$F_2 = tanh({arg_2}^2) \tag{21}$$

$$arg_2 = max\left(2\frac{\sqrt{k}}{0.09\omega y};\frac{500\nu}{y^2\omega}\right) \tag{22}$$

As mentioned earlier in the paper, pseudo-transient approach is applied to calculate steady state temperature field. The reason for choosing pseudo-transient approach is to make sure that our written CFD code is capable of solving transient equations correctly. It should be noted that the PDEs we will encounter in inverse analysis section are all in transient form. Energy equation in its transient form is written as follows,

$$\frac{\partial}{\partial t}(\rho T) + \frac{\partial}{\partial x}(\rho u T) + \frac{\partial}{\partial y}(\rho v T) = \frac{\partial}{\partial x}\left(\Gamma_{eff}\frac{\partial T}{\partial x}\right) + \frac{\partial}{\partial y}\left(\Gamma_{eff}\frac{\partial T}{\partial y}\right) \tag{23}$$

Eq. (23) is called time-average transport equation for scalar T in which variable Γ_{eff} denotes effective diffusivity and is expressed as,

$$\Gamma_{eff} = \frac{k_{th}}{c_p} + \frac{\mu_t}{\sigma_t} \tag{24}$$

The variable σ_t is called Prandtl-Schmidt dimensionless number which is assumed to be equal to 1.0 in most numerical procedures used in computational fluid dynamics [18]. Pseudo-transient time step size (Δt_{PT}) can be obtained through the following expression,

$$(1-\alpha_T)\frac{a_P}{\alpha_T} = \frac{\rho \Delta V}{\Delta t_{PT}} \tag{25}$$

In Eq. (25), α_T, a_P, ΔV, and ρ are under-relaxation factor used while solving discretised energy equation in its steady state form, central coefficient of the discretised equation, volume of cells, and density of the fluid respectively. The boundary conditions for the foregoing partial differential equations are as follows,

$$u = U_{in} \quad v = V_{in} = 0 \quad k = k_{in} \quad \omega = \omega_{in} \quad T = T_{in} \quad at\ x = 0 \tag{26}$$

$$\frac{\partial u}{\partial x} = \frac{\partial v}{\partial x} = \frac{\partial k}{\partial x} = \frac{\partial \omega}{\partial x} = \frac{\partial T}{\partial x} = 0 \quad at\ x = L \tag{27}$$

$$u = v = 0 \quad k = k_w \quad \omega = \omega_w \quad \left(\Gamma_{eff}\frac{\partial T}{\partial y}\right) = \frac{q''_w(x,t)}{c_p} \quad at\ y = 0 \tag{28}$$

$$\frac{\partial u}{\partial y} = \frac{\partial k}{\partial y} = \frac{\partial \omega}{\partial y} = \frac{\partial T}{\partial y} = 0 \quad v = 0 \quad at\ y = r_0 \tag{29}$$

It should be noted that dimensional wall heat flux is defined as follows,

$$q''_w(x,t) = \begin{cases} \dfrac{Q''_{w_1}(\xi)k_{th}T_{in}}{D} & for\ x \le L/2 \\ \dfrac{Q''_{w_2}(\xi)k_{th}T_{in}}{D} & for\ x > L/2 \end{cases} \tag{30}$$

In Eq. (30), $Q''_{w_1}(\xi)$ and $Q''_{w_2}(\xi)$ are dimensionless wall heat fluxes and ξ denotes dimensionless time which is expressed by

$$\xi = \frac{tU_{in}}{2r_0} \tag{31}$$

Turbulence quantities (k, ω) can be roughly calculated at the inlet and on the wall of the channel through the following expressions [19,20],

$$k_{in} = \frac{3}{2}(U_{in}I)^2 \tag{32}$$

$$\omega_{in} = \frac{{k_{in}}^{1/2}}{{c_\mu}^{1/4}(0.07D)} \tag{33}$$

$$k_w = 0 \qquad \omega_w = \frac{60\nu}{\beta_1\left(\Delta y_p\right)^2} \tag{34}$$

In the present research, the physical domain of the problem (Figure 1) is discretised into quadrilateral cells. Figure (2) indicates the effect of the number of cells used in the numerical calculation on steady state fully-developed Nusselt number. According to Figure (2), when the number of cells used in the numerical procedure rises above 160000, no change is observed in the value of steady state fully-developed Nusselt number. Table (1) compares exact values of steady state fully-developed Nusselt number and wall shear stress with those numerically obtained in this paper. According to Table (1), the calculated quantities of interest obtained by the present code are in good agreement with their analytical counterparts.

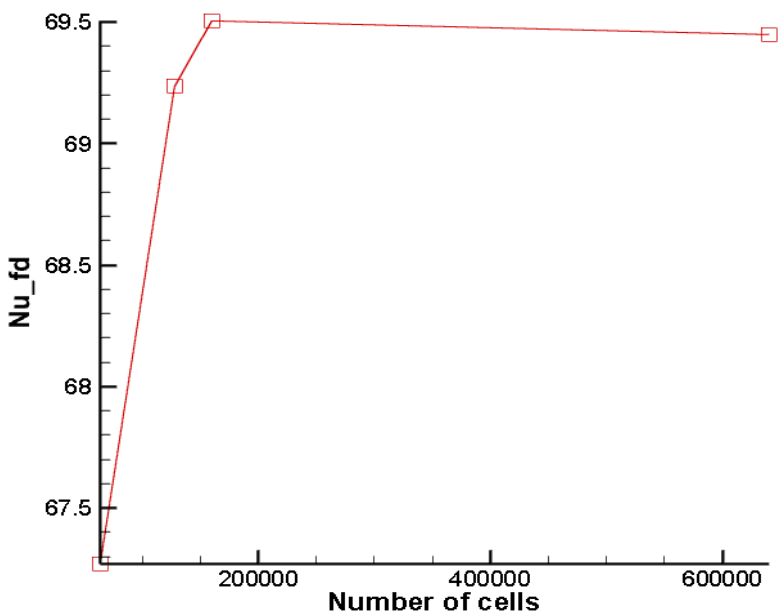

Figure 2 Grid study graph

Table 1 Comparison of the calculated quantities of interest with other references.

Quantity of interest	Exact value	Present study	Relative error
Nu_{fd}	69.73 (Colburn formula)	69.5025	0.003262
τ_w (Pa)	0.0393 (Blasius formula)	0.03687223	0.06177

Figure (3) shows the flow chart of the SIMPLE algorithm used in the present research in order to solve pressure-velocity coupling.

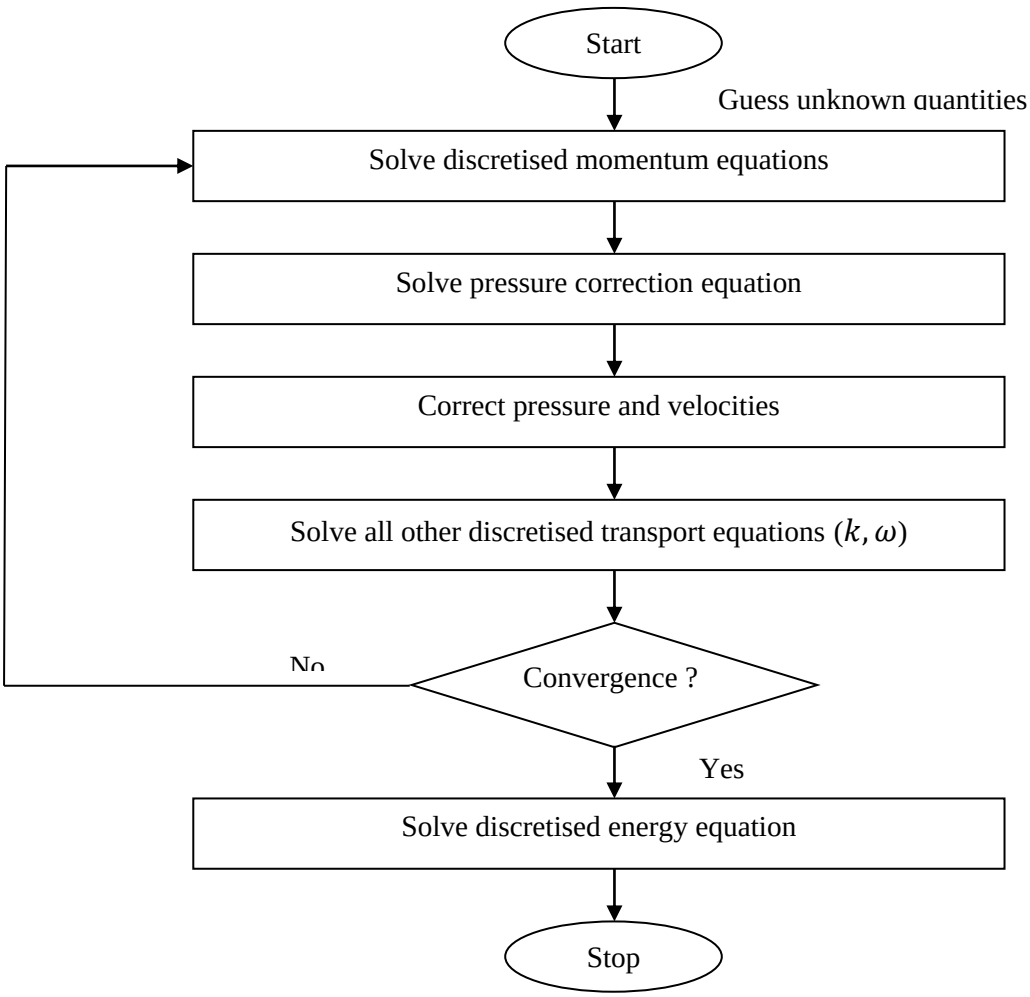

Figure 3 The SIMPLE algorithm used in the present paper to solve pressure-velocity coupling

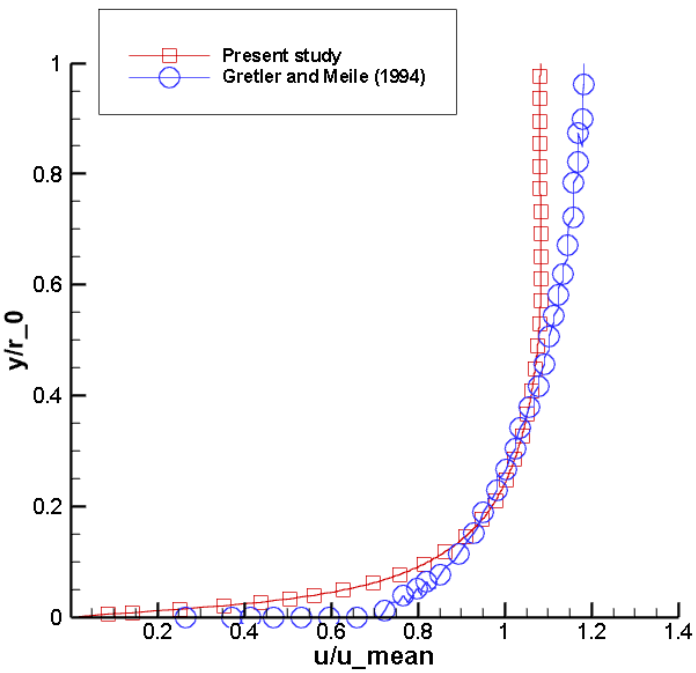

Figure 4 Comparison of the fully-developed velocity profile obtained through the present code with Gretler and Meile predictions [21]

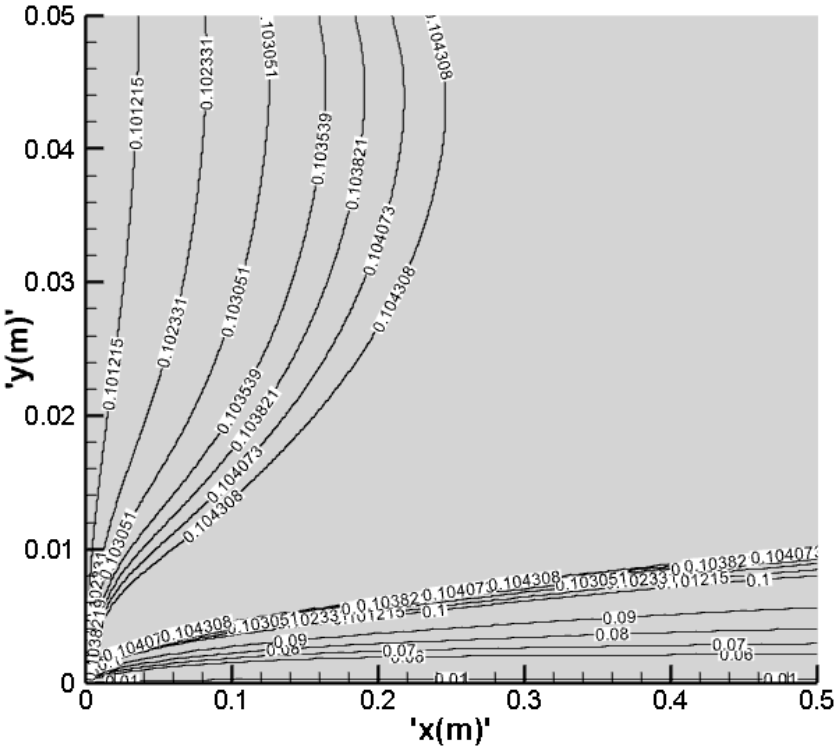

Figure 5 u-velocity isolines at the inlet of the channel

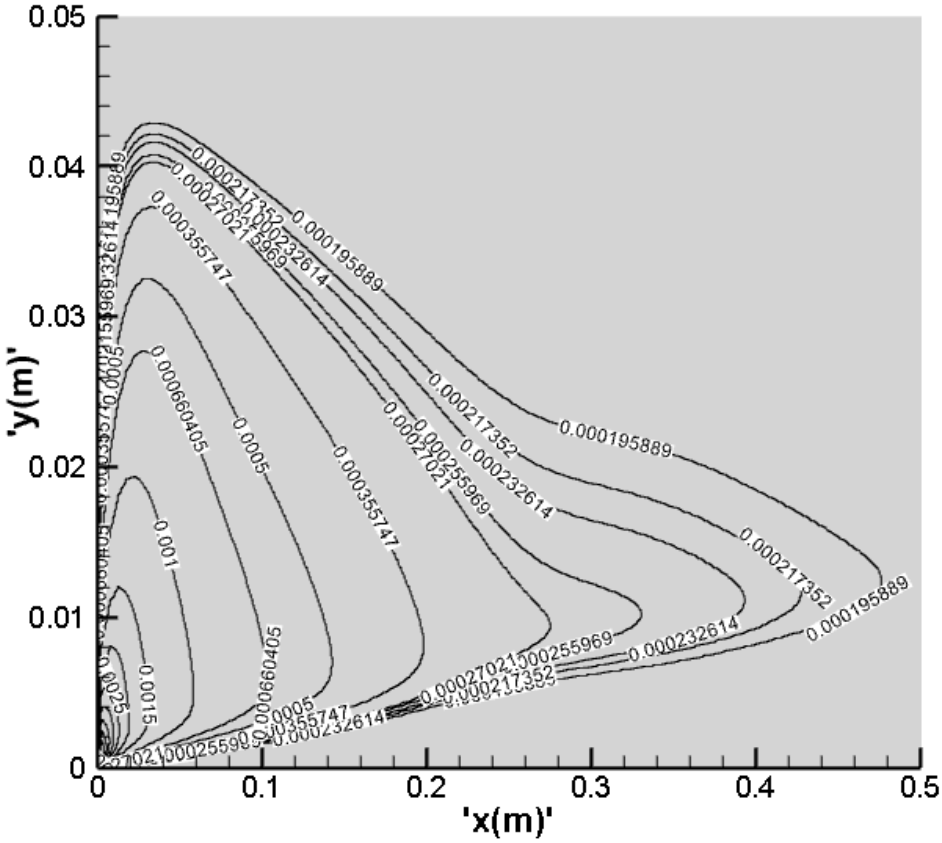

Figure 6 v-velocity isolines at the inlet of the channel

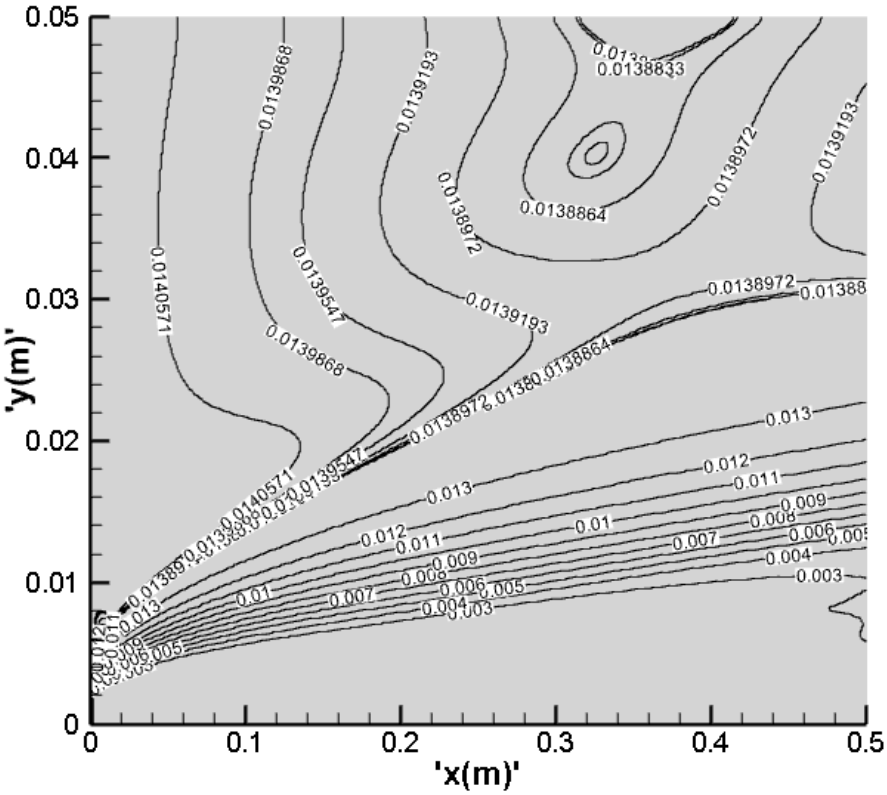

Figure 7 Eddy viscosity isolines at the inlet of the channel

According to Figure (4), fully-developed velocity profile calculated by numerical simulation is in good agreement with Gretler and Meile predictions [21]. Figures (5)-(7) show u-velocity, v-velocity, and eddy viscosity isolines respectively at the inlet of the channel obtained through the paper's CFD code.

3 Inverse convection problem

According to Figure (1), the purpose of the inverse analysis is to estimate the heat fluxes applied to the channel's wall simultaneously with the help of temperature measurements in sensors' locations on the wall. There are various methods of formulating an inverse problem, but conjugate gradient method (CGM) with adjoint problem is used in this study. Main advantage of the above-mentioned method is that it has no need of calculating sensitivity matrix which is a time-consuming process. The first step in formulating an inverse problem is to specify the objective function. In actual fact, wall heat flux estimation is conducted through objective function minimisation. In the inverse analysis, objective function is defined as follows [22],

$$S\left(Q''_{w_1}(\xi), Q''_{w_2}(\xi)\right) = \sum_{m=1}^{M} \int_{\xi=\xi_0}^{\xi_f} \left[Z_m(\xi) - \theta(X_m, Y_m, \xi; Q''_{w_1}(\xi), Q''_{w_2}(\xi))\right]^2 d\xi \tag{35}$$

In Eq. (35), $Z_m(\xi)$, $\theta(X_m, Y_m, \xi; Q''_{w_1}(\xi), Q''_{w_2}(\xi))$, and M denote dimensionless measured temperature, dimensionless estimated temperature, and total number of sensors respectively. In order to develop direct, sensitivity, and adjoint problems, the following dimensionless parameters are applied

$$\theta = \frac{T}{T_{in}} \quad U = \frac{u}{U_{in}} \quad V = \frac{v}{U_{in}} \quad X = \frac{x}{2r_0} \quad Y = \frac{y}{2r_0} \quad \Lambda = \frac{\Gamma_{eff}}{\mu} \tag{36}$$

3.1 Direct problem

In this research, direct problem of the inverse analysis is defined as follows,

$$\frac{\partial}{\partial \xi}(\theta) + \frac{\partial}{\partial X}(U\theta) + \frac{\partial}{\partial Y}(V\theta) = \frac{1}{Re}\left[\frac{\partial}{\partial X}\left(\Lambda \frac{\partial \theta}{\partial X}\right) + \frac{\partial}{\partial Y}\left(\Lambda \frac{\partial \theta}{\partial Y}\right)\right] \tag{37.a}$$

$$\theta = 1 \quad at\ X = 0 \tag{37.b}$$

$$\frac{\partial \theta}{\partial Y} = -Q''_{w_1}(\xi) \quad at\ Y = 0, for\ 0 \le X \le \frac{L}{4r_0}, \qquad \xi > \xi_0 \tag{37.c}$$

$$\frac{\partial \theta}{\partial Y} = -Q''_{w_2}(\xi) \quad at\ Y = 0, for\ X > \frac{L}{4r_0}, \qquad \xi > \xi_0 \tag{37.d}$$

$$\frac{\partial \theta}{\partial Y} = 0 \quad at\ Y = \frac{1}{2} \tag{37.e}$$

$$\frac{\partial \theta}{\partial X} = 0 \quad at\ X = \frac{L}{2r_0} \tag{37.f}$$

$$\theta = 1 \quad for\ \xi = \xi_0 \tag{37.g}$$

The direct problem defined by Eqs. 37 is concerned with the determination of the dimensionless temperature field $\theta(X, Y, \xi)$, when dimensionless wall heat fluxes $Q''_{w_1}(\xi), Q''_{w_2}(\xi)$ are known.

3.2 Sensitivity problem

The sensitivity function $\Delta\theta(X, Y, \xi)$**,** solution of the sensitivity problem, is defined as the directional derivative of the temperature $\theta(X, Y, \xi)$ in the direction of the perturbation of the unknown functions [22]. The sensitivity function is needed for the computation of the search step sizes, as will be apparent later in the paper. The sensitivity problem can be obtained by assuming that the temperature $\theta(X, Y, \xi)$ is perturbed by an amount $\Delta\theta(X, Y, \xi)$, when the unknown wall heat fluxes $Q''_{w_1}(\xi), Q''_{w_2}(\xi)$ are perturbed by $\Delta Q''_{w_1}(\xi), \Delta Q''_{w_2}(\xi)$ respectively. By replacing $\theta(X, Y, \xi)$ by $[\theta(X, Y, \xi) + \Delta\theta(X, Y, \xi)]$, $Q''_{w_1}(\xi)$ by $\left[Q''_{w_1}(\xi) + \Delta Q''_{w_1}(\xi)\right]$, and $Q''_{w_2}(\xi)$ by $\left[Q''_{w_2}(\xi) + \Delta Q''_{w_2}(\xi)\right]$ in the direct problem given by Eqs. (37), and then subtracting the original direct problem from the resulting expressions, the following sensitivity problem is obtained:

$$\frac{\partial}{\partial \xi}(\Delta\theta) + \frac{\partial}{\partial X}(U\Delta\theta) + \frac{\partial}{\partial Y}(V\Delta\theta) = \frac{1}{Re}\left[\frac{\partial}{\partial X}\left(\Lambda \frac{\partial \Delta\theta}{\partial X}\right) + \frac{\partial}{\partial Y}\left(\Lambda \frac{\partial \Delta\theta}{\partial Y}\right)\right] \tag{38.a}$$

$$\Delta\theta = 0 \quad at\ X = 0 \tag{38.b}$$

$$\frac{\partial \Delta\theta}{\partial Y} = -\Delta Q''_{w_1}(\xi) \quad at\ Y = 0, for\ 0 \le X \le \frac{L}{4r_0}, \qquad \xi > \xi_0 \tag{38.c}$$

$$\frac{\partial \Delta\theta}{\partial Y} = -\Delta Q''_{w_2}(\xi) \quad at\ Y = 0, for\ X > \frac{L}{4r_0}, \qquad \xi > \xi_0 \tag{38.d}$$

$$\frac{\partial \Delta\theta}{\partial Y} = 0 \quad at\ Y = \frac{1}{2} \tag{38.e}$$

$$\frac{\partial \Delta\theta}{\partial X} = 0 \quad at\ X = \frac{L}{2r_0} \tag{38.f}$$

$$\Delta\theta = 0 \quad for\ \xi = \xi_0 \tag{38.g}$$

3.3 Adjoint problem

A Lagrange multiplier $\lambda(X, Y, \xi)$ comes into picture in the minimisation of the function (35) because the temperature $\theta(X_m, Y_m, \xi; Q''_{w_1}(\xi), Q''_{w_2}(\xi))$ appearing in such function needs to satisfy a constraint, which is the solution of the direct problem. Such Lagrange multiplier, needed for the computation of the gradient equations (as will be apparent later), is obtained through the solution of a problem adjoint to the sensitivity problem given by Eqs. (38).
The boundary value problem for the Lagrange multiplier $\lambda(X, Y, \xi)$ is defined as follows,

$$\frac{\partial}{\partial \xi}(\lambda) + \frac{\partial}{\partial X}(U\lambda) + \frac{\partial}{\partial Y}(V\lambda) + \frac{1}{Re}\left[\frac{\partial}{\partial X}\left(\Lambda\frac{\partial \lambda}{\partial X}\right) + \frac{\partial}{\partial Y}\left(\Lambda\frac{\partial \lambda}{\partial Y}\right)\right] + 2\sum_{m=1}^{M}\left[\theta(X_m, Y_m, \xi; Q''_{w_1}(\xi), Q''_{w_2}(\xi)) - Z_m(\xi)\right] = 0 \tag{39.a}$$

$$\lambda = 0 \quad at\ X = 0 \tag{39.b}$$

$$\frac{\partial \lambda}{\partial Y} = 0 \quad at\ Y = 0 \tag{39.c}$$

$$\frac{\partial \lambda}{\partial Y} = 0 \quad at\ Y = \frac{1}{2} \tag{39.d}$$

$$\lambda = 0\ , \frac{\partial \lambda}{\partial X} = 0 \quad at\ X = \frac{L}{2r_0} \tag{39.e}$$

$$\lambda = 0 \quad for\ \xi = \xi_f \tag{39.f}$$

For more information on how to derive the adjoint problem, the reader should consult reference [22]. It should be noted that in the adjoint problem, the condition (39.f) is the value of the function $\lambda(X, Y, \xi)$ at the final time $\xi = \xi_f$. In the conventional initial value problem, the value of the function is specified at time $\xi = \xi_0$. However, the final value problem (39) can be transformed into an initial value problem by defining a new time variable given by $\zeta = \xi_f - \xi$.

3.4 Gradient equations

The purpose of solving the adjoint problem is to calculate gradient equations used in the inverse analysis. In this study, gradient equations are defined by the following relations,

$$\nabla S\left(Q''_{w_1}(\xi)\right) = \frac{1}{Re}\int_{X=0}^{L/(4r_0)} \lambda(X,0,\xi) \times \Lambda(X,0)dX \tag{40.a}$$

$$\nabla S\left(Q''_{w_2}(\xi)\right) = \frac{1}{Re}\int_{X=L/(4r_0)}^{L/(2r_0)} \lambda(X,0,\xi) \times \Lambda(X,0)dX \tag{40.b}$$

3.5 The iterative procedure for CGM with adjoint problem

The iterative procedure of the conjugate gradient method (CGM) with adjoint problem, for the computation of the unknown wall heat fluxes $Q''_{w_1}(\xi), Q''_{w_2}(\xi)$, is given by the following equations,

$$Q''^{\,iter+1}_{w_1}(\xi) = Q''^{\,iter}_{w_1}(\xi) - Beta_1^{\,iter} \times dod_1^{\,iter}(\xi) \tag{41.a}$$

$$Q''^{\,iter+1}_{w_2}(\xi) = Q''^{\,iter}_{w_2}(\xi) - Beta_2^{\,iter} \times dod_2^{\,iter}(\xi) \tag{41.b}$$

$$dod_1^{\,iter}(\xi) = \nabla S\left(Q''^{\,iter}_{w_1}(\xi)\right) + \Upsilon_1^{\,iter} dod_1^{\,iter-1}(\xi) \tag{42.a}$$

$$dod_2^{\,iter}(\xi) = \nabla S\left(Q''^{\,iter}_{w_2}(\xi)\right) + \Upsilon_2^{\,iter} dod_2^{\,iter-1}(\xi) \tag{42.b}$$

$$\Upsilon_1^{\,iter} = \frac{\int_{\xi=\xi_0}^{\xi_f} \nabla S\left(Q''^{\,iter}_{w_1}(\xi)\right)\left\{\nabla S\left(Q''^{\,iter}_{w_1}(\xi)\right) - \nabla S\left(Q''^{\,iter-1}_{w_1}(\xi)\right)\right\} d\xi}{\int_{\xi=\xi_0}^{\xi_f} \left\{\nabla S\left(Q''^{\,iter-1}_{w_1}(\xi)\right)\right\}^2 d\xi} \tag{43.a}$$

$$\Upsilon_2^{\,iter} = \frac{\int_{\xi=\xi_0}^{\xi_f} \nabla S\left(Q''^{\,iter}_{w_2}(\xi)\right)\left\{\nabla S\left(Q''^{\,iter}_{w_2}(\xi)\right) - \nabla S\left(Q''^{\,iter-1}_{w_2}(\xi)\right)\right\} d\xi}{\int_{\xi=\xi_0}^{\xi_f} \left\{\nabla S\left(Q''^{\,iter-1}_{w_2}(\xi)\right)\right\}^2 d\xi} \tag{43.b}$$

The search step sizes $Beta_1^{\,iter}, Beta_2^{\,iter}$ are chosen as the ones that minimise the objective function (35) at each iteration [22]. The purpose of solving the sensitivity problem is to calculate search step sizes used in the inverse analysis. In this study, search step sizes are defined by the following relations,

$$Beta_1^{\,iter} = \frac{G_1 H_{22} - G_2 H_{12}}{H_{11}H_{22} - H_{12}^{\,2}} \tag{44.a}$$

$$Beta_2^{\,iter} = \frac{G_2 H_{11} - G_1 H_{12}}{H_{11}H_{22} - H_{12}^{\,2}} \tag{44.b}$$

Where

$$G_1 = \sum_{m=1}^{M} \int_{\xi=\xi_0}^{\xi_f} \left[\theta\left(X_m, Y_m, \xi; Q''^{\,iter}_{w_1}(\xi), Q''^{\,iter}_{w_2}(\xi)\right) - Z_m(\xi)\right] \Delta\theta\left(X_m, Y_m, \xi; dod_1^{\,iter}(\xi)\right) d\xi \tag{45.a}$$

$$G_2 = \sum_{m=1}^{M} \int_{\xi=\xi_0}^{\xi_f} \left[\theta\left(X_m, Y_m, \xi; Q''_{w_1}{}^{iter}(\xi), Q''_{w_2}{}^{iter}(\xi)\right) - Z_m(\xi)\right] \Delta\theta\left(X_m, Y_m, \xi; dod_2{}^{iter}(\xi)\right) d\xi \tag{45.b}$$

$$H_{11} = \sum_{m=1}^{M} \int_{\xi=\xi_0}^{\xi_f} \left[\Delta\theta\left(X_m, Y_m, \xi; dod_1{}^{iter}(\xi)\right)\right]^2 d\xi \tag{45.c}$$

$$H_{22} = \sum_{m=1}^{M} \int_{\xi=\xi_0}^{\xi_f} \left[\Delta\theta\left(X_m, Y_m, \xi; dod_2{}^{iter}(\xi)\right)\right]^2 d\xi \tag{45.d}$$

$$H_{12} = \sum_{m=1}^{M} \int_{\xi=\xi_0}^{\xi_f} \left[\Delta\theta\left(X_m, Y_m, \xi; dod_1{}^{iter}(\xi)\right)\right] \times \left[\Delta\theta\left(X_m, Y_m, \xi; dod_2{}^{iter}(\xi)\right)\right] d\xi \tag{45.e}$$

Further details on the derivation of Eqs. (44) can be found in reference [22].

3.6 The stopping criterion for CGM with adjoint problem

The stopping criterion for conjugate gradient method with adjoint problem is based on the discrepancy principle, when the standard deviation σ of the measurements is a priori known. It is given by

$$S\left(Q''_{w_1}(\xi), Q''_{w_2}(\xi)\right) < \varepsilon \tag{46}$$

Where $S\left(Q''_{w_1}(\xi), Q''_{w_2}(\xi)\right)$ is computed with Eq. (35). The tolerance ε is then obtained from Eq. (35) by assuming

$$\sigma \approx |Z(\xi) - \theta(\xi)| \tag{47}$$

Where σ is the standard deviation of the measurement errors, which is assumed to be constant. Thus, the tolerance ε is determined as

$$\varepsilon = M\sigma^2\xi_f \tag{48}$$

For cases involving errorless measurements, ε can be specified a priori as a sufficiently small number.

3.7 The computational algorithm for CGM with adjoint problem

The computational algorithm for CGM with adjoint problem can be summarised as follows,
Step 1. Make an initial guess for the unknown wall heat fluxes.
Step 2. Solve the direct problem (37) in order to calculate $\theta(X, Y, \xi)$.
Step 3. Check the stopping criterion (46). Continue if not satisfied.
Step 4. Solve the adjoint problem (39) in order to compute $\lambda(X, 0, \xi)$.

Step 5. Knowing $\lambda(X,0,\xi)$, compute gradients of the objective function from Eqs. (40).
Step 6. Knowing the gradients, compute conjugation coefficients from Eqs. (43) and the directions of descent from Eqs. (42).
Step 7. Set $\Delta Q''_{w_1}(\xi) = dod_1^{iter}(\xi), \Delta Q''_{w_2}(\xi) = dod_2^{iter}(\xi)$ and solve the sensitivity problem (38) to obtain $\Delta\theta\left(X_m, Y_m, \xi; dod_1^{iter}(\xi)\right), \Delta\theta\left(X_m, Y_m, \xi; dod_2^{iter}(\xi)\right)$.
Step 8. Knowing $\Delta\theta\left(X_m, Y_m, \xi; dod_1^{iter}(\xi)\right), \Delta\theta\left(X_m, Y_m, \xi; dod_2^{iter}(\xi)\right)$, compute the search step sizes from Eqs. (44).
Step 9. Knowing the search step sizes and the directions of descent, compute the new estimates from Eqs. (41), and return to step 2.

4 Solution of the partial differential equations

The foregoing partial differential equations are solved numerically using finite volume method with the help of first order upwind differencing scheme. SIMPLE algorithm is utilised to obtain steady state flow field in this study. Successive over-relaxation method is used in order to solve linear systems of equations. It should be noted that staggered grid is applied in the present numerical simulation. Furthermore, for the purpose of discretising transient terms, fully implicit scheme is used. The codes for both direct and inverse parts of the research have been written in Fortran programming language.

5 Results

According to Figure (1), for the purpose of simultaneously estimating step heat flux functions applied to the channel's wall, 4 different arrangements of the sensors on the wall are examined. The main objective is to study the effect of sensors' arrangement and the number of sensors at each half of the channel's wall on the accuracy of estimations. Step heat flux functions are defined as follows,

$$Q''_{w_1}(\xi) = \begin{cases} 0 & if\ \xi = \xi_0 \\ 4 & if\ \xi_1 \le \xi \le \xi_{50} \\ 3 & if\ \xi_{51} \le \xi \le \xi_{100} \\ 5 & if\ \xi_{101} \le \xi \le \xi_{150} \\ 1 & if\ \xi_{151} \le \xi \le \xi_{200} \end{cases} \tag{49.a}$$

$$Q''_{w_2}(\xi) = \begin{cases} 0 & if\ \xi = \xi_0 \\ 1 & if\ \xi_1 \le \xi \le \xi_{50} \\ 3 & if\ \xi_{51} \le \xi \le \xi_{100} \\ 2 & if\ \xi_{101} \le \xi \le \xi_{150} \\ 5 & if\ \xi_{151} \le \xi \le \xi_{200} \end{cases} \tag{49.b}$$

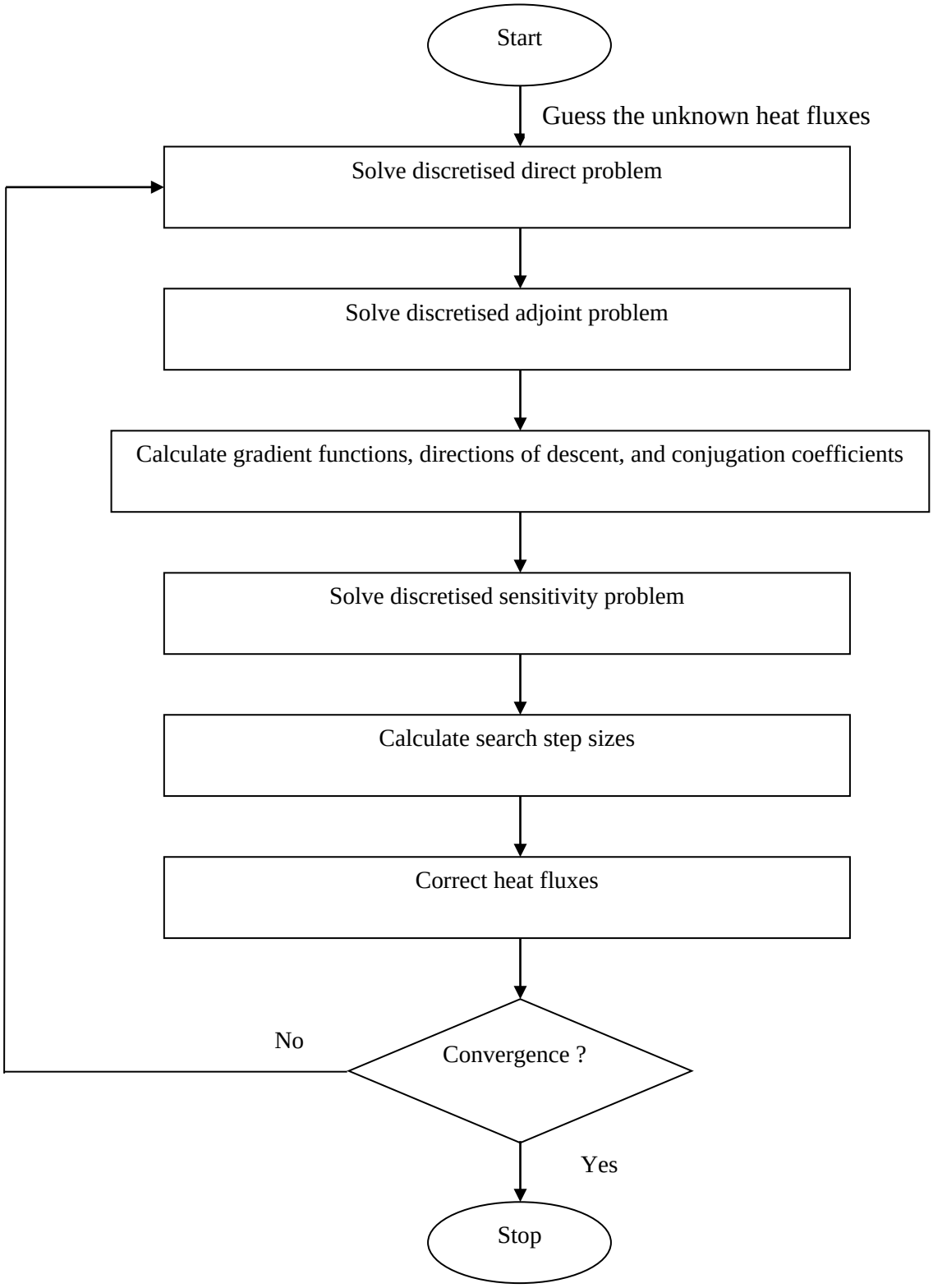

Figure 8 The CGM algorithm

Figure (8) indicates the flow chart of the CGM algorithm used for inverse analysis in the present research.

5.1 Results of the first arrangement of the sensors

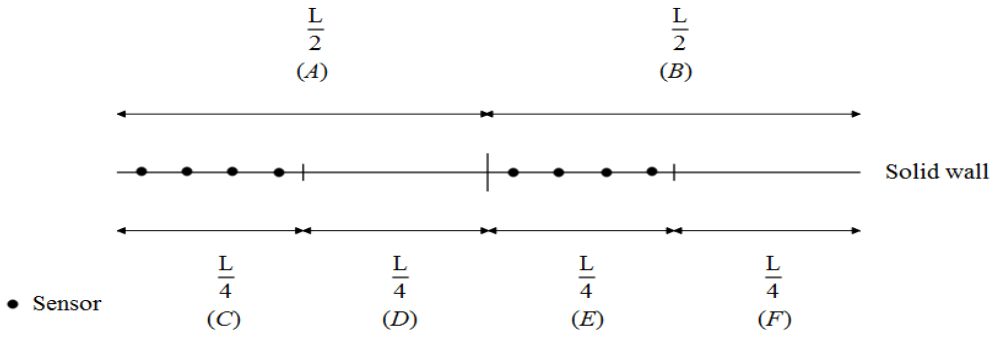

Figure 9-a 1st arrangement of the sensors

According to Figure (9-a), the number of sensors at the 1st and 3rd quarters of the channel's wall are considered to be equal to M_A and M_B respectively. Spaces between the sensors at each quarter are taken to be equal.

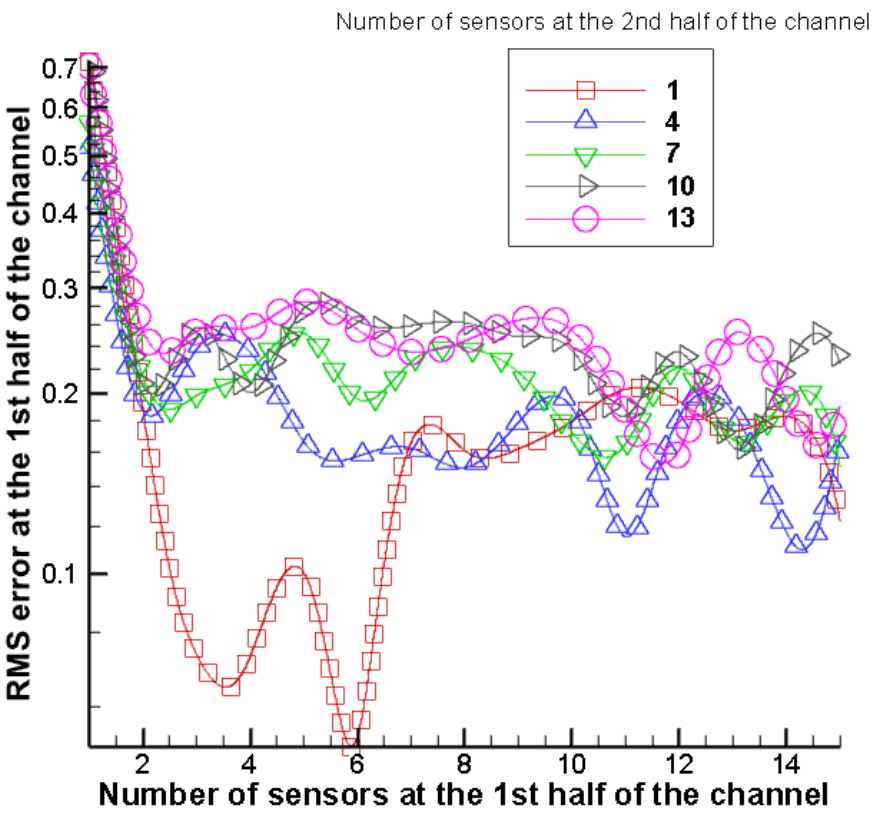

Figure 9-b RMS error at the 1st half of the channel's wall

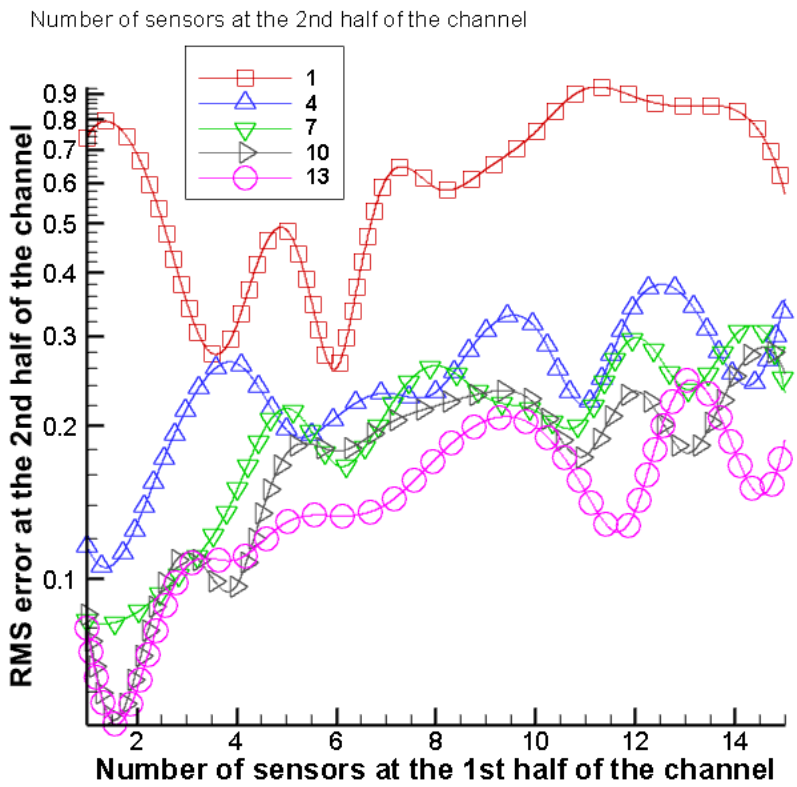

Figure 9-c RMS error at the 2nd half of the channel's wall

Figures (9-b) and (9-c) indicate the values of RMS error at each half of the channel for different number of sensors at each half. It should be noted that RMS error could be calculated by the following expression [22],

$$(RMS\ error)_m = \frac{\sqrt{\frac{1}{NoT}\sum_{i=1}^{NoT}\left[Q''_{w_{est_m}}(\xi_i) - Q''_{w_{ex_m}}(\xi_i)\right]^2}}{\sqrt{\frac{1}{NoT}\sum_{i=1}^{NoT}\left[Q''_{w_{ex_m}}(\xi_i)\right]^2}},\ \ for\ m = 1,2 \tag{50}$$

5.2 Results of the second arrangement of the sensors

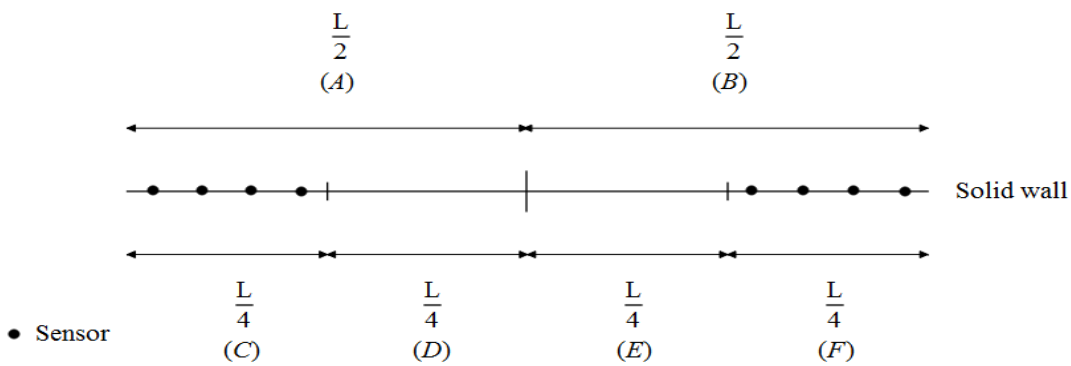

Figure 10-a 2nd arrangement of the sensors

According to Figure (10-a), the number of sensors at the 1st and 4th quarters of the channel's wall are considered to be equal to M_A and M_B respectively. Spaces between the sensors at each quarter are taken to be equal.

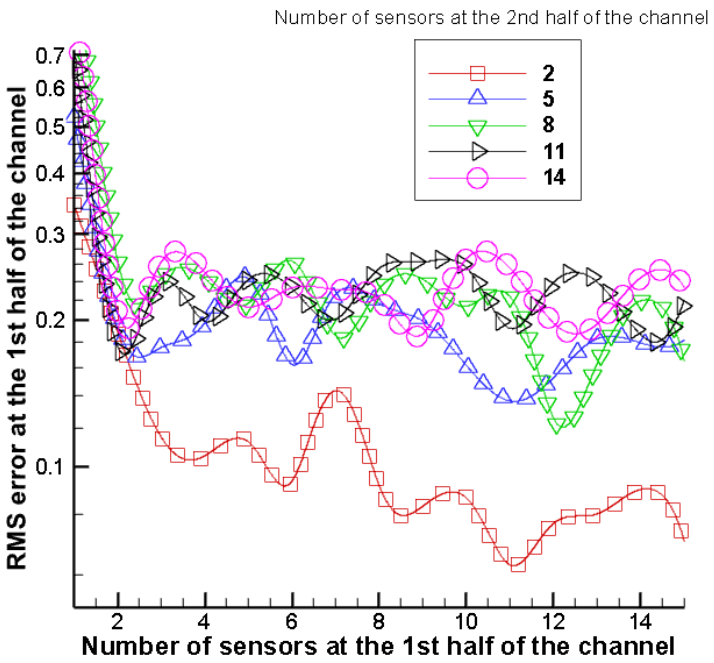

Figure 10-b RMS error at the 1st half of the channel's wall

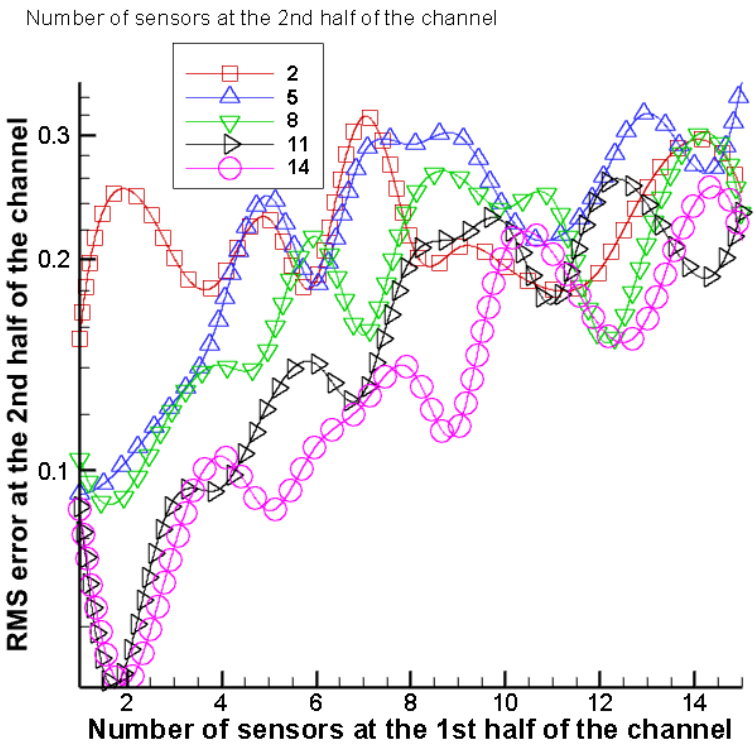

Figure 10-c RMS error at the 2nd half of the channel's wall

Figures (10-b) and (10-c) indicate the values of RMS error at each half of the channel for different number of sensors at each half.

5.3 Results of the third arrangement of the sensors

According to Figure (11-a), the number of sensors at the 2nd and 3rd quarters of the channel's wall are considered to be equal to M_A and M_B respectively. Spaces between the sensors at each quarter are taken to be equal.

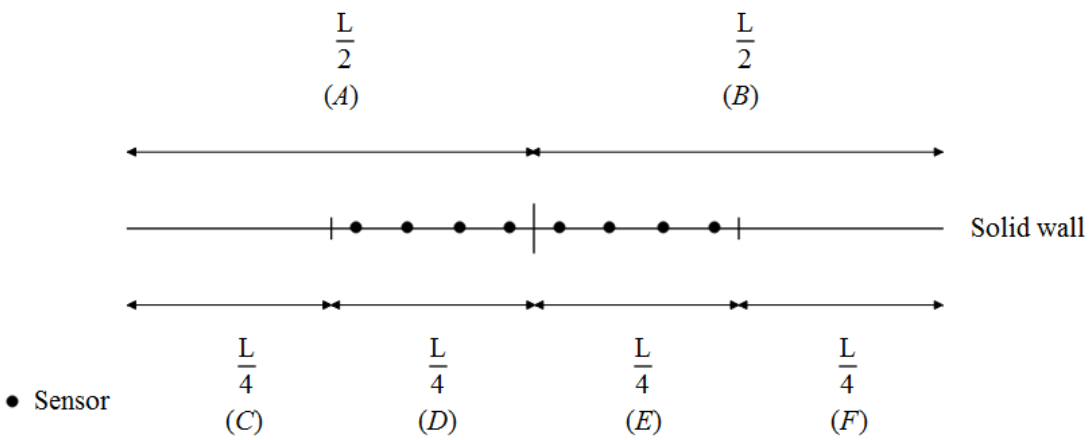

Figure 11-a 3rd arrangement of the sensors

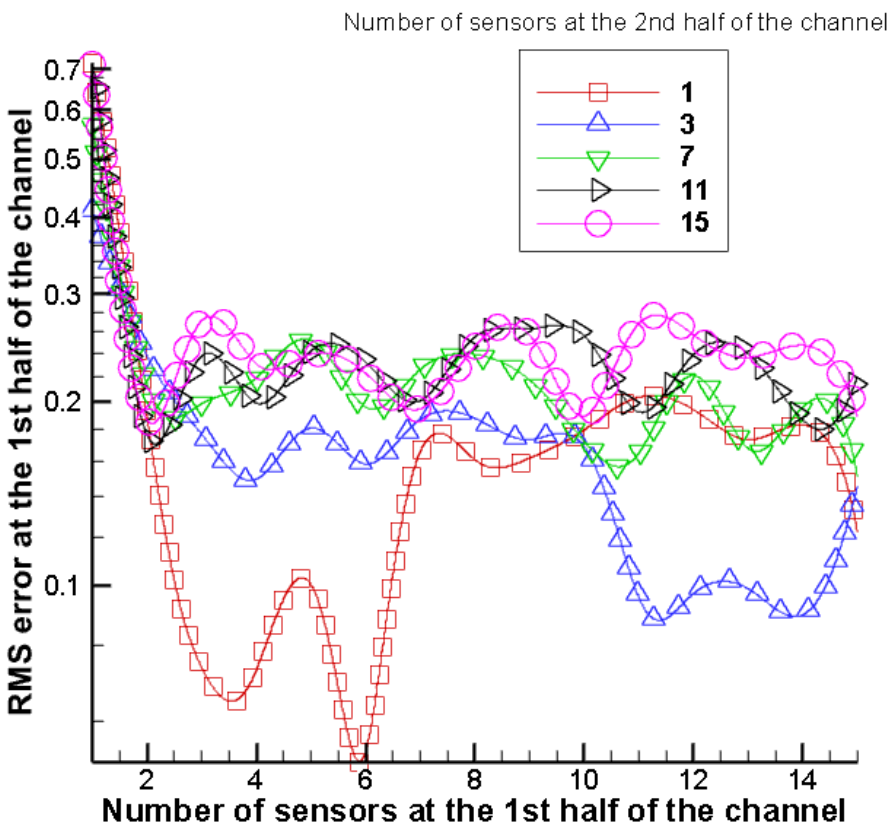

Figure 11-b RMS error at the 1st half of the channel's wall

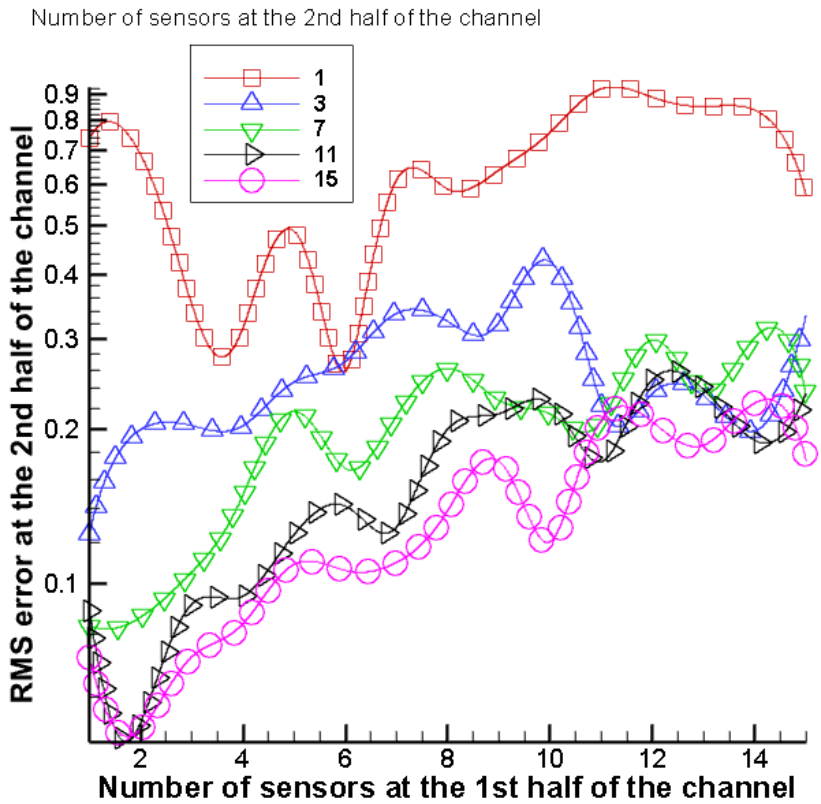

Figure 11-c RMS error at the 2nd half of the channel's wall

Figures (11-b) and (11-c) indicate the values of RMS error at each half of the channel for different number of sensors at each half.

5.4 Results of the fourth arrangement of the sensors

According to Figure (12-a), the number of sensors at the 2nd and 4th quarters of the channel's wall are considered to be equal to M_A and M_B respectively. Spaces between the sensors at each quarter are taken to be equal.

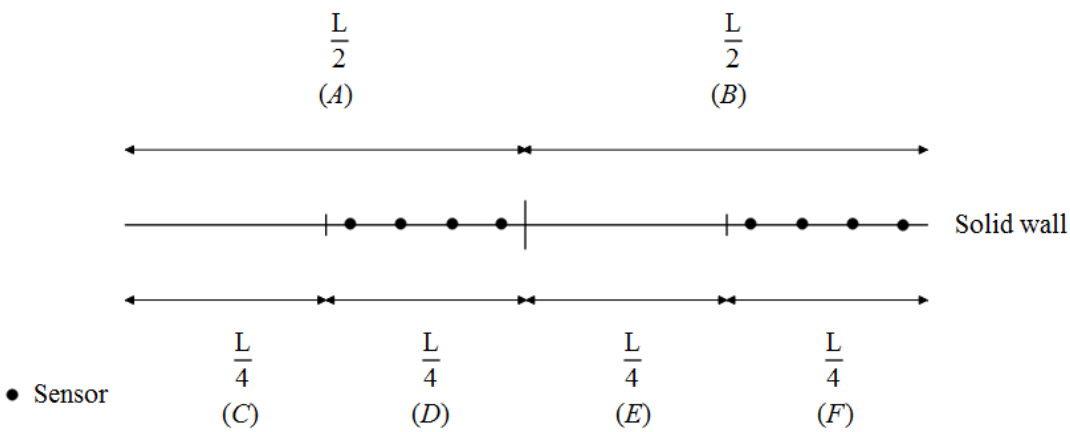

Figure 12-a 4th arrangement of the sensors

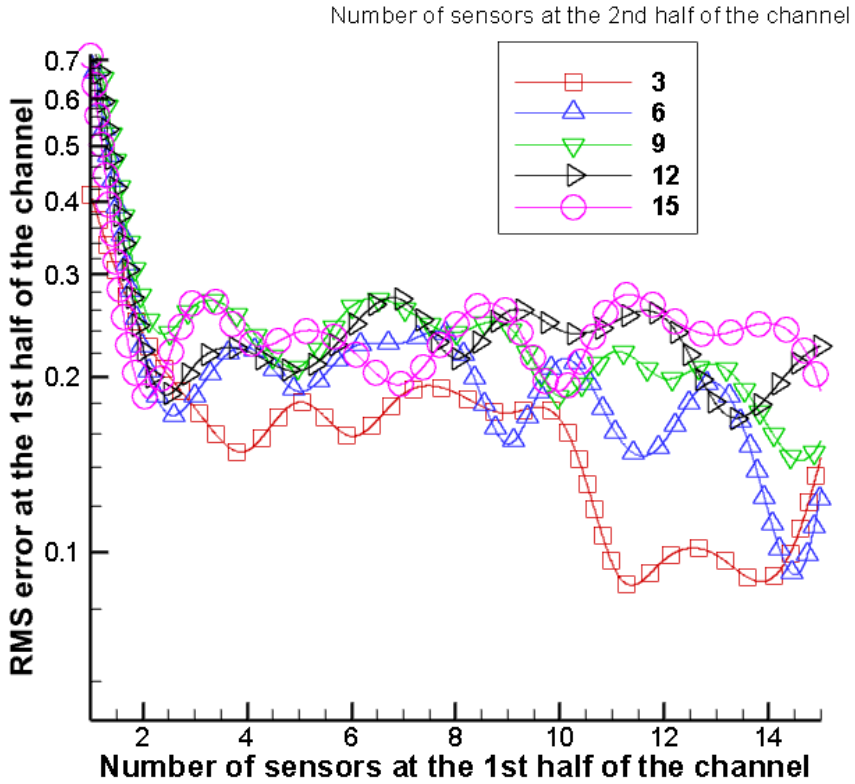

Figure 12-b RMS error at the 1st half of the channel's wall

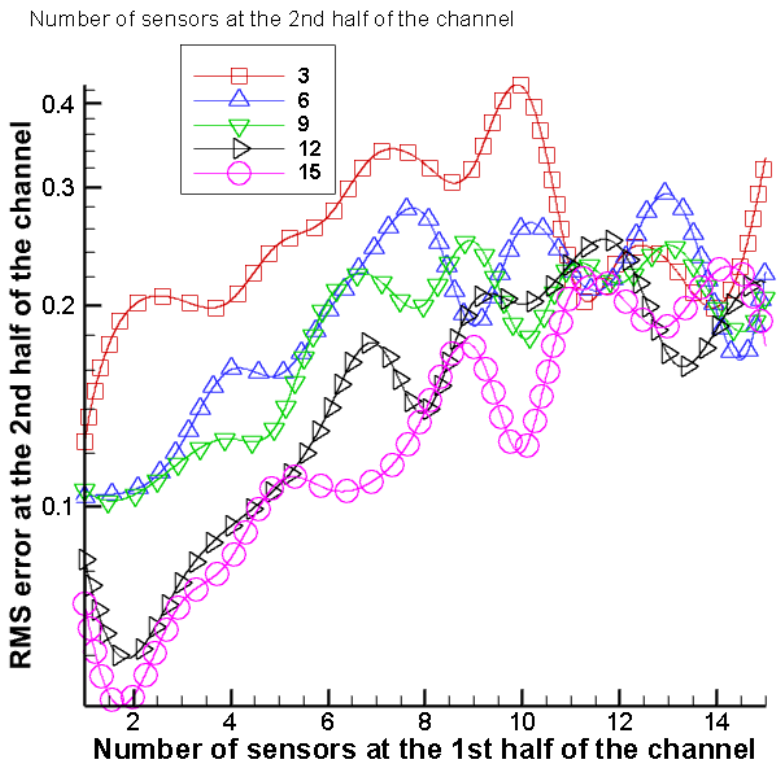

Figure 12-c RMS error at the 2nd half of the channel's wall

Figures (12-b) and (12-c) indicate the values of RMS error at each half of the channel for different number of sensors at each half.

5.5 Deciding optimum cases from the examined ones

With the help of the foregoing results indicated in sections (5.1)-(5.4), it is possible to determine optimum cases in terms of sensors' arrangement and the number of sensors at each half of the channel's wall. The results show that choosing the 2nd arrangement of the sensors and the number of sensors at the 1st and 2nd halves of the channel's wall respectively equal to 12 and 8, the most accurate estimations can be obtained for the step heat flux functions applied to the channel's wall. Table (2) indicates 4 optimum cases based on RMS errors.

Table 2 The most optimum cases based on RMS errors.

#	Arrangement of the sensors	M_A	M_B	RMS_A	RMS_B
1	2nd	12	8	0.1259	0.1544
2	1st	12	13	0.1610	0.1367
3	2nd	3	5	0.1785	0.1254
4	1st	2	4	0.1874	0.1281

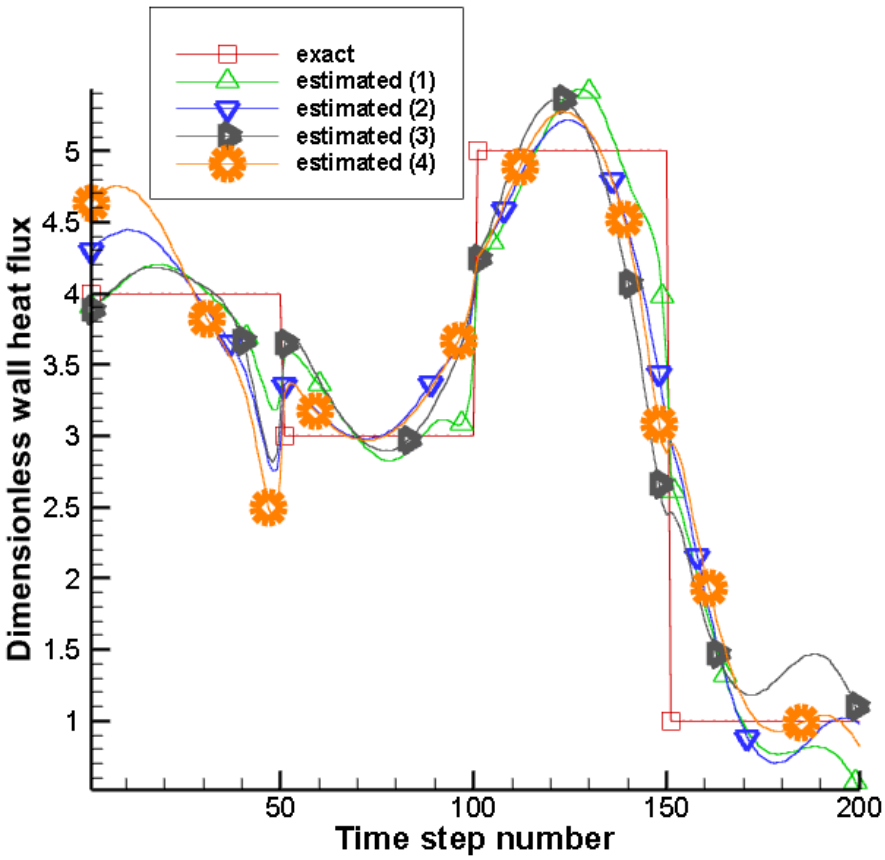

Figure 13-a Comparison of the exact and estimated heat fluxes at the 1st half of the channel's wall

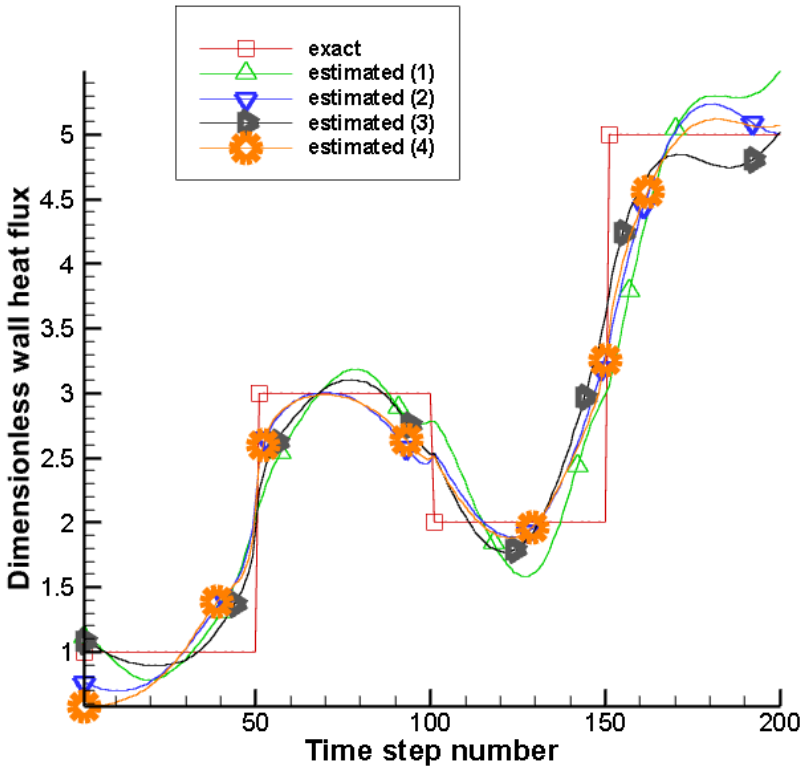

Figure 13-b Comparison of the exact and estimated heat fluxes at the 2nd half of the channel's wall

Figures (13-a) and (13-b) compare the exact heat flux with the estimated ones at the 1st and 2nd halves of the channel's wall respectively. Cases (1)-(4) indicated in Figures (13-a) and (13-b) are relating to the above-mentioned cases in Table (2). Figures (14-a) and (14-b) compare the exact temperature profile with the estimated ones at the 1st and 2nd halves of the channel's wall respectively. Figure (15) shows convergence history for case (1) in Table (2). It should be mentioned that the foregoing results are related to errorless data used in the inverse analysis. In order to conduct an inverse analysis using noisy data, the following expression is used to produce noisy data [22],

$$Z_{noisy}(\xi_i) = Z(\xi_i) + \Psi\sigma \tag{51}$$

In Eq. (51), $Z_{noisy}(\xi_i), Z(\xi_i), \sigma,$ and Ψ are called noisy temperature of the sensors, errorless temperature of the sensors, standard deviation of the measurement errors, and random variable with normal distribution respectively. For the 99% confidence level, one should consider $-2.576 < \Psi < 2.576$ [22].

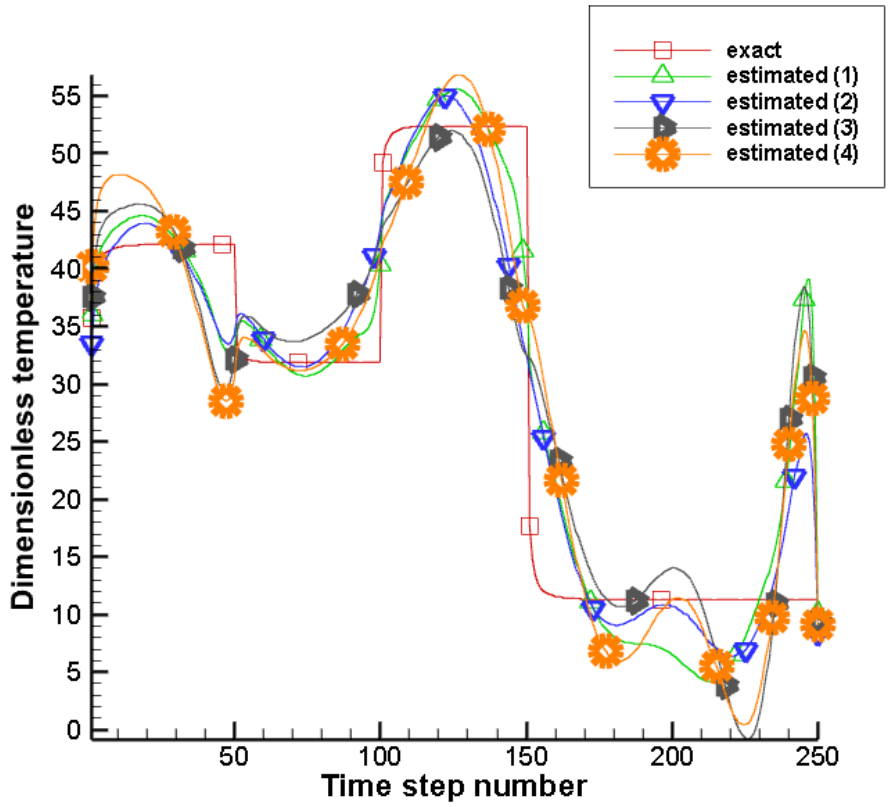

Figure 14-a Comparison of the exact and estimated temperature profiles at the 1st half of the channel's wall

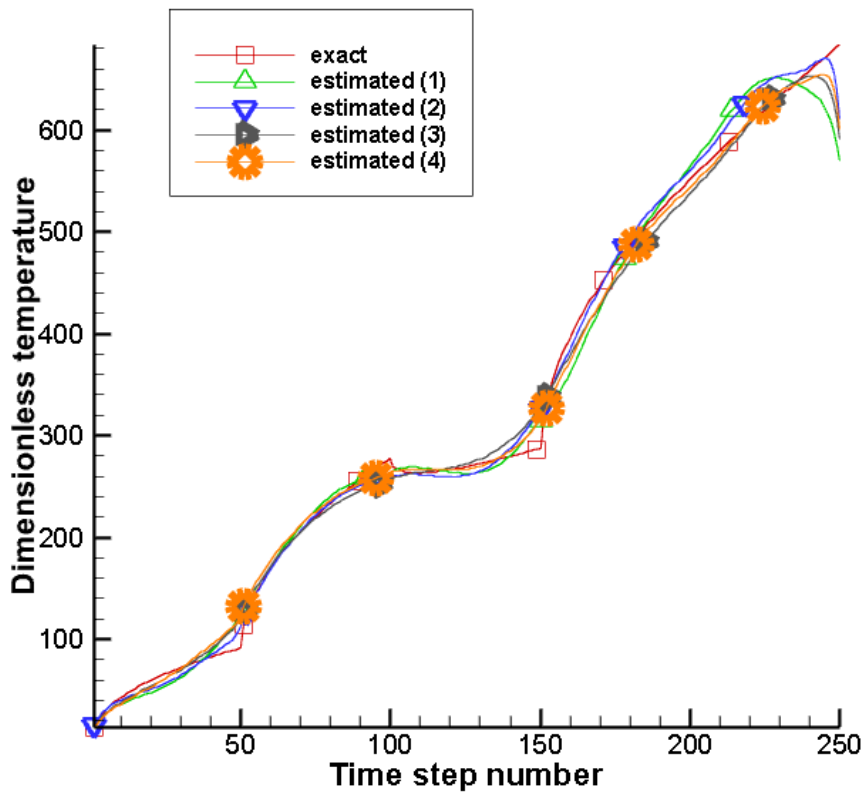

Figure 14-b Comparison of the exact and estimated temperature profiles at the 2nd half of the channel's wall

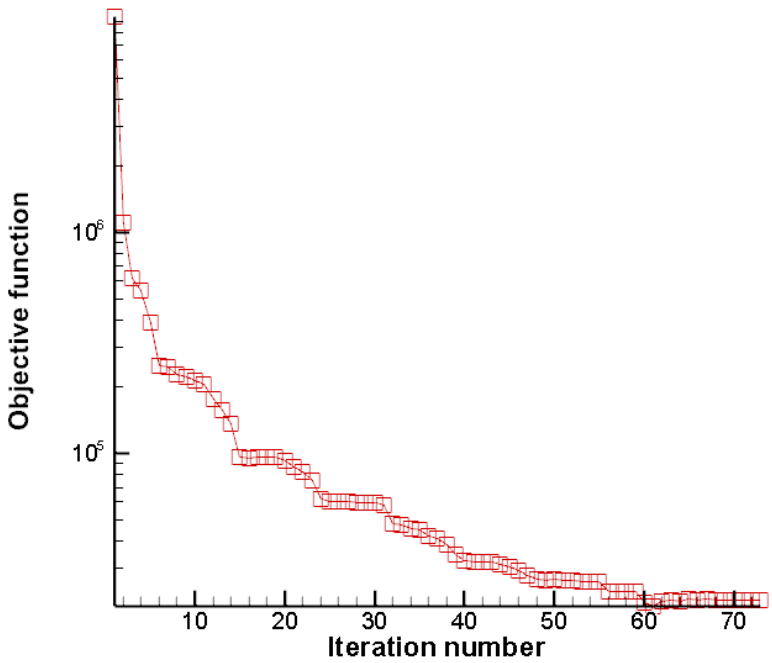

Figure 15 Convergence history for case (1) in Table (2)

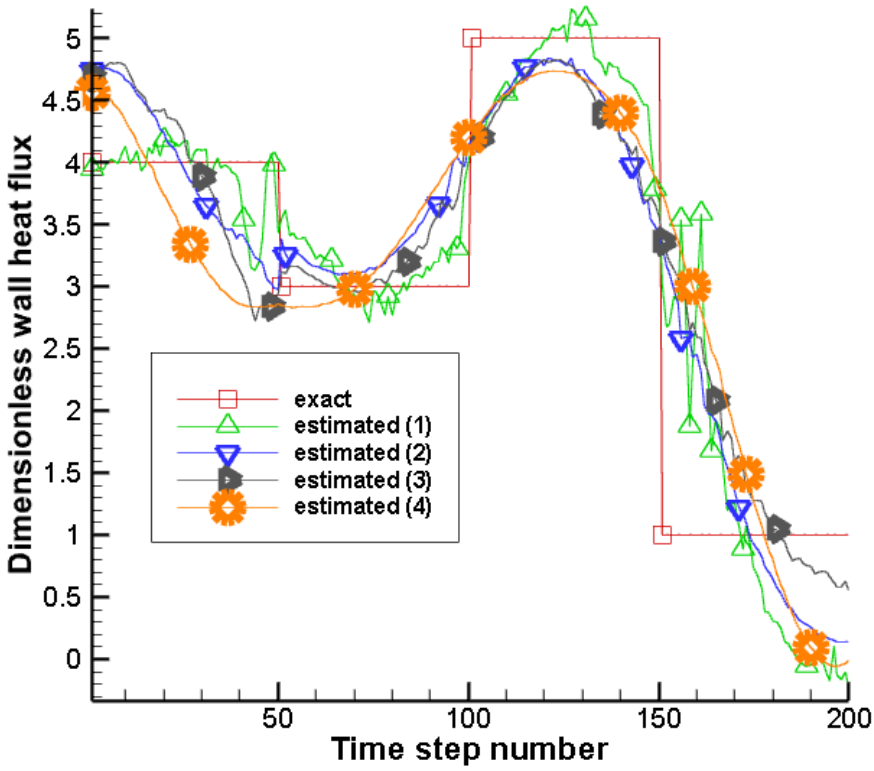

Figure 16-a Comparison of the exact and estimated heat fluxes at the 1st half of the channel's wall (noisy data)

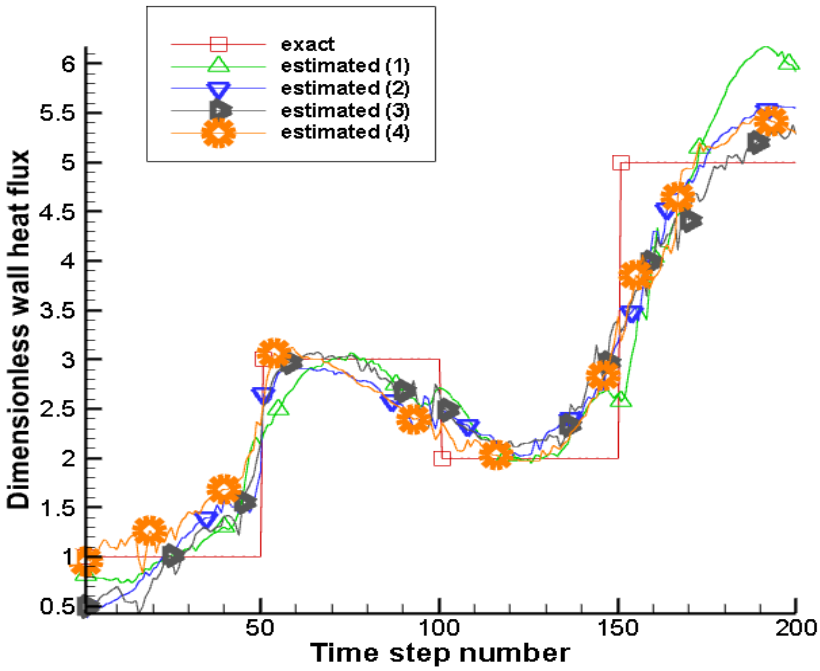

Figure 16-b Comparison of the exact and estimated heat fluxes at the 2nd half of the channel's wall (noisy data)

Figures (16-a) and (16-b) compare the exact heat flux with the estimated ones at the 1st and 2nd halves of the channel's wall respectively using noisy data. Cases (1)-(4) indicated in Figures (16-a) and (16-b) are relating to the above-mentioned cases in Table (2).
Figures (17-a) and (17-b) compare the exact temperature profile with the estimated ones at the 1st and 2nd halves of the channel's wall respectively using the noisy data for the case (1) indicated in Table (2). Figure (18) shows convergence history of the inverse analysis for case (1) in Table (2) using noisy data.

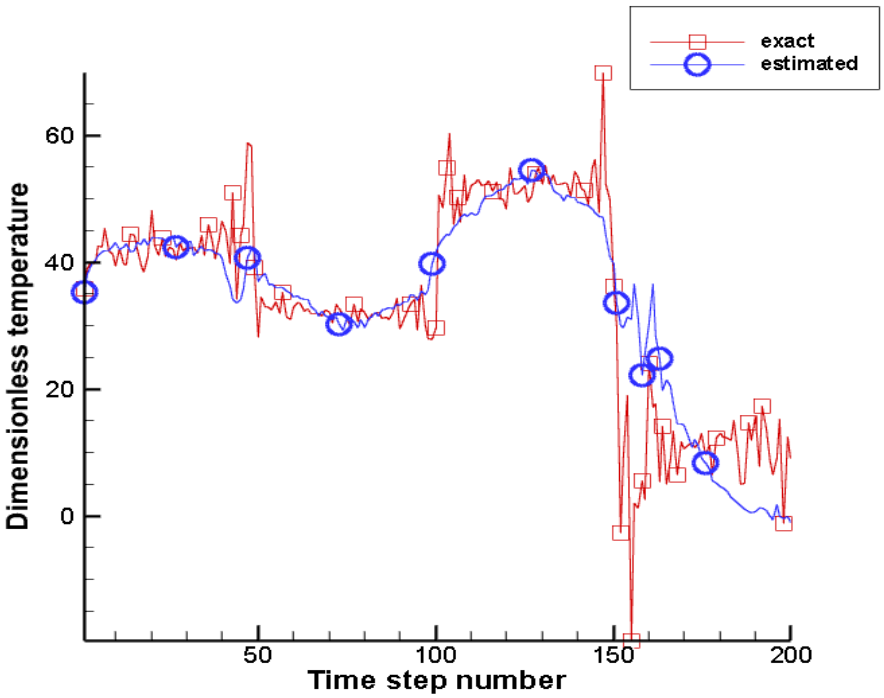

Figure 17-a Comparison of the exact and estimated temperature profiles at the 1st half of the channel's wall (noisy data)

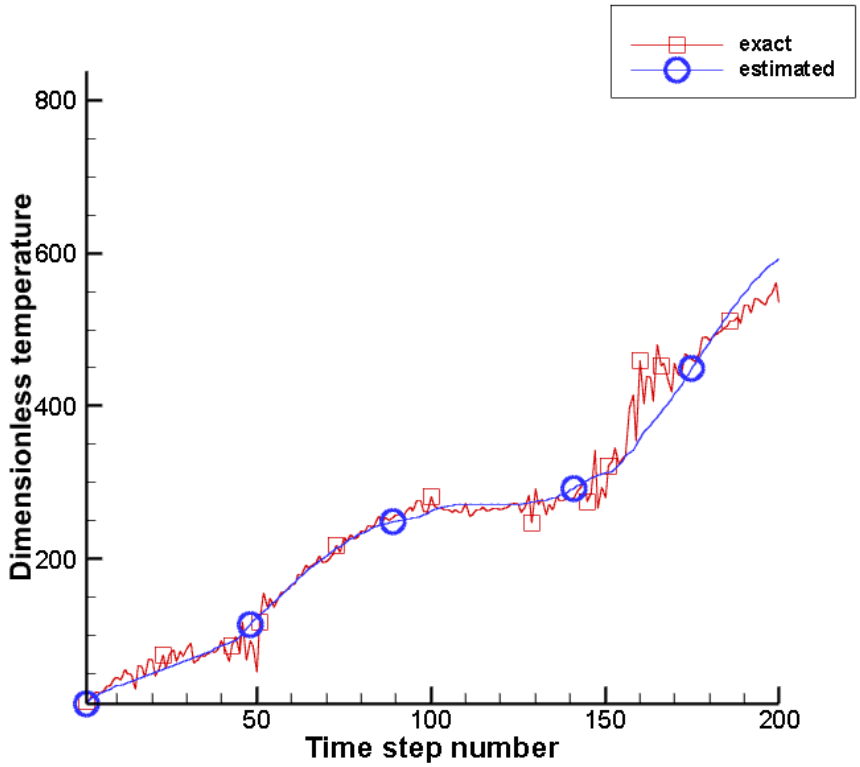

Figure 17-b Comparison of the exact and estimated temperature profiles at the 2nd half of the channel's wall (noisy data)

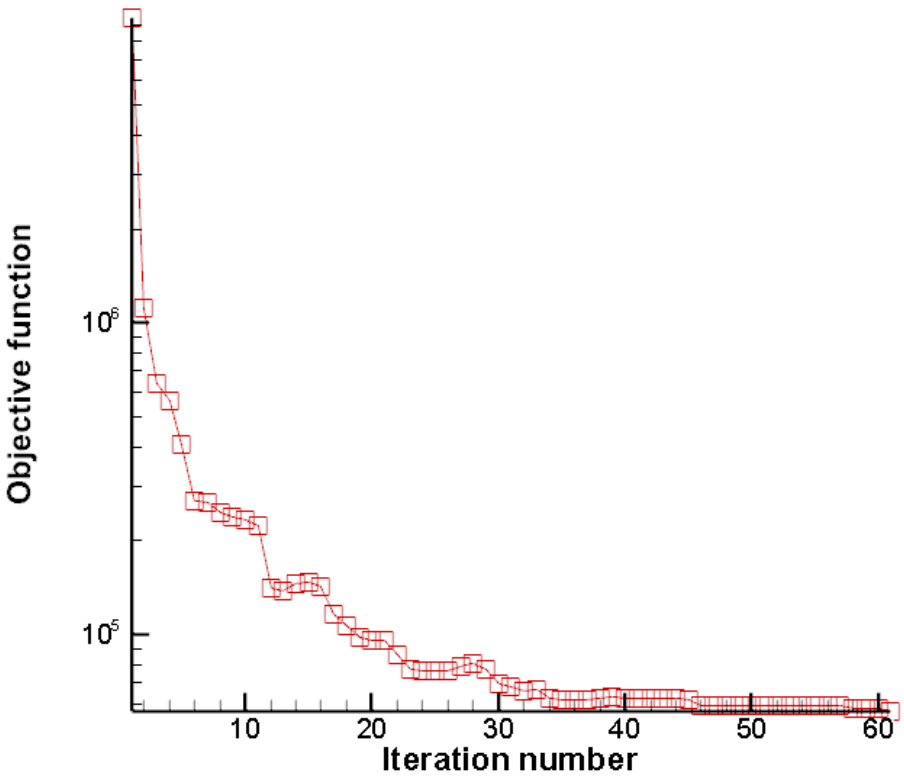

Figure 18 Convergence history for case (1) in Table (2) (noisy data)

6 Discussion and conclusion

In this study, step heat fluxes applied to the wall of a two-dimensional symmetric channel with turbulent flow were estimated simultaneously using conjugate gradient method with adjoint problem. $SST\ k-\omega$ turbulence model was used for simulating steady state flow field. In order to validate the numerically obtained flow field, wall shear stress, fully-developed velocity profile, and steady state nusselt number were compared with their counterparts available in the literature. For inverse analysis, temperature simulated measurements were taken from the sensors placed on the channel's wall. The main objective was to examine the effect of the number of sensors and their arrangement on the wall upon the accuracy of the estimations. The results indicated that the most optimum case based on RMS errors could be obtained by applying the 2nd arrangement of the sensors. The most suitable number of sensors at the 1st and 2nd halves of the wall was decided to be equal to 12 and 8 respectively. With the help of errorless data for the inverse analysis, RMS errors at the 1st and 2nd halves of the wall became equal to 0.1259 and 0.1544 respectively. On the other hand, if noisy data were used for the inverse analysis, RMS errors at the 1st and 2nd halves of the wall would be equal to 0.1854 and 0.2037 respectively. For both errorless and noisy cases, the results of the inverse analysis were validated by comparing exact and estimated functions. It should be noted that according to the validations, the proposed inverse method has been capable of simultaneously estimating the unknown wall heat fluxes with acceptable accuracy.
The developed methodology for simultaneously estimating the unknown wall heat fluxes in a turbulent channel flow is general and could be applied to other inverse turbulent forced convection problem in identifying boundary conditions. Furthermore, the main innovate aspect of the present study was to find out ideal length of the channel's wall on which sensors are located.

References

[1] Huang, C.H., and Chen, W.C., "A Three-dimensional Inverse Forced Convection Problem in Estimating Surface Heat Flux by Conjugate Gradient Method", International Journal of Heat and Mass Transfer, Vol. 43, pp. 3171-3181, 2000/09/01/ (2000).

[2] Li, H.Y., and Yan, W.M., "Inverse Convection Problem for Determining Wall Heat Flux in Annular Duct Flow", Journal of Heat Transfer, Vol. 122, pp. 460-464, (2000).

[3] Colaco, M.J., and Orlande, H.R.B., "Inverse Forced Convection Problem of Simultaneous Estimation of Two Boundary Heat Fluxes in Irregularly Shaped Channels", Numerical Heat Transfer, Part A: Applications, Vol. 39, pp. 737-760, 2001/05/25 (2001).

[4] Prud'homme, M., and Nguyen, T.H., "Solution of Inverse Free Convection Problems by Conjugate Gradient Method: Effects of Rayleigh Number", International Journal of Heat and Mass Transfer, Vol. 44, pp. 2011-2027, 2001/06/01/ (2001).

[5] Kim, S.K., Lee, W.I., and Lee, J.S., "Solving a Nonlinear Inverse Convection Problem using the Sequential Gradient Method", KSME International Journal, Vol. 16, pp. 710-719, 2002/05/01 (2002).

[6] Kim, S.K., and Lee, W.I.L., "An Inverse Method for Estimating Thermophysical Properties of Fluid Flowing in a Circulating Duct", International Communications in Heat and Mass Transfer, Vol. 29, pp. 1029-1036, 2002/11/01/ (2002).

[7] Hong, Y.K., and Baek, S.W., "Inverse Analysis for Estimating the Unsteady Inlet Temperature Distribution for Two-phase Laminar Flow in a Channel", International Journal of Heat and Mass Transfer, Vol. 49, pp. 1137-1147, 2006/03/01/ (2006).

[8] Chen, C.O.K., Wu, L.W., and Yang, Y.T., "Comparison of Whole-domain and Sequential Algorithms for Function Specification Method in the Inverse Heat Transfer Problem of Laminar Convective Pipe Flow", Numerical Heat Transfer, Part A: Applications, Vol. 50, pp. 927-947, 2006/12/01 (2006).

[9] Lin, D.T.W., Yan, W.M., and Li, H.Y., "Inverse Problem of Unsteady Conjugated Forced Convection in Parallel Plate Channels", International Journal of Heat and Mass Transfer, Vol. 51, pp. 993-1002, 2008/03/01/ (2008).

[10] Zhao, F.Y., Liu, D., Tang, L., Ding, Y.L., and Tang, G.F., "Direct and Inverse Mixed Convections in an Enclosure with Ventilation Ports", International Journal of Heat and Mass Transfer, Vol. 52, pp. 4400-4412, 2009/09/01/ (2009).

[11] Zhao, F.Y., Liu, D., and Tang, G.F., "Determining Boundary Heat Flux Profiles in an Enclosure Containing Solid Conducting Block", International Journal of Heat and Mass Transfer, Vol. 53, pp. 1269-1282, 2010/03/01/ (2010).

[12] Parwani, A.K., Talukdar, P., and Subbarao, P.M.V., "Estimation of Inlet Temperature of a Developing Fluid Flow in a Parallel Plate Channel", International Journal of Thermal Sciences, Vol. 57, pp. 126-134, 2012/07/01/ (2012).

[13] Moghadassian, B., and Kowsary, F., "Inverse Boundary Design Problem of Natural Convection–radiation in a Square Enclosure", International Journal of Thermal Sciences, Vol. 75, pp. 116-126, 2014/01/01/ (2014).

[14] Zhang, D.D., Zhang, J.H., Liu, D., Zhao, F.Y., Wang, H.Q., and Li, X.H., "Inverse Conjugate Heat Conduction and Natural Convection Inside an Enclosure with Multiple Unknown Wall Heating Fluxes", International Journal of Heat and Mass Transfer, Vol. 96, pp. 312-329, 2016/05/01/ (2016).

[15] Min, C., Li, X., Yuan, Y., Chen, Z., and Tian, L., "An Inverse Study to Optimize the Rib Pitch in a Two–dimensional Channel Flow Problem for Heat Transfer Enhancement", International Journal of Heat and Mass Transfer, Vol. 112, pp. 1044-1051, 2017/09/01/ (2017).

[16] Bangian-Tabrizi, A., and Jaluria, Y., "An Optimization Strategy for the Inverse Solution of a Convection Heat Transfer Problem", International Journal of Heat and Mass Transfer, Vol. 124, pp. 1147-1155, 2018/09/01/ (2018).

[17] Hafid, M., and Lacroix, M., "Inverse Method for Simultaneously Estimating Multi-parameters of Heat Flux and of Temperature-dependent Thermal Conductivities inside Melting Furnaces", Applied Thermal Engineering, Vol. 141, pp. 981-989, 2018/08/01/ (2018).

[18] Versteeg, H.K., and Malalasekera, W., "*An Introduction to Computational Fluid Dynamics*", The Finite Volume Method: Pearson Education Limited, Harlow, England, (2007).

[19] Menter, F.R., "Two-equation Eddy-viscosity Turbulence Models for Engineering Applications", AIAA Journal, Vol. 32, pp. 1598-1605, 1994/08/01 (1994).

[20] F. Inc., Fluent 6.3 User's Guide: Fluent Inc., (2006).

[21] Gretler, W., and Meile, W., "Shear Stress Calculation in Asymmetric Turbulent Flows: a Combined ARS-model", Fluid Dynamics Research, Vol. 14, pp. 289-311, 1994/12 (1994).

[22] Ozisik, M.N, "*Inverse Heat Transfer: Fundamentals and Applications*", Taylor & Francis, (2000).

Nomenclature

c_p	Specific heat capacity ($\frac{J}{kg.K}$)
dod	Direction of descent
D	Height of the channel (m)
I	Turbulence intensity
k	Kinetic turbulence energy ($\frac{m^2}{s^2}$)
k_{th}	Thermal conductivity ($\frac{W}{m.K}$)
L	Length of the channel (m)
M	Number of sensors
NoT	Number of time steps
Nu_{fd}	Nusselt number
p	Pressure (Pa)
q''_w	Wall heat flux ($\frac{W}{m^2}$)
Q''_w	Dimensionless wall heat flux
RMS	Root-mean-square error
Re	Reynolds number
r_0	Half of the channel's height (m)
S	Objective function
T	Temperature (K)
t	Time (s)
u, v	Velocity components ($\frac{m}{s}$)
x, y	Cartesian coordinates (m)
Z	Dimensionless measurement

Greek symbols

βeta	Search step size
$\Delta\theta$	Sensitivity function
$\Delta Q''_w$	Perturbed wall heat flux
Δy_p	Distance to the next point away from the wall (m)

λ	Lagrange multiplier
σ	Standard deviation
Υ	Conjugation coefficient
Ψ	Random variable
ω	Turbulence frequency ($\frac{1}{s}$)
Ω	Mean vorticity ($\frac{1}{s}$)

Subscripts

A	1st half of the channel's wall
B	2nd half of the channel's wall
est	Estimated
ex	Exact
f	Final time
in	Inlet of the channel
w	Wall of the channel
0	Initial time

Superscripts

$iter$	Iteration number